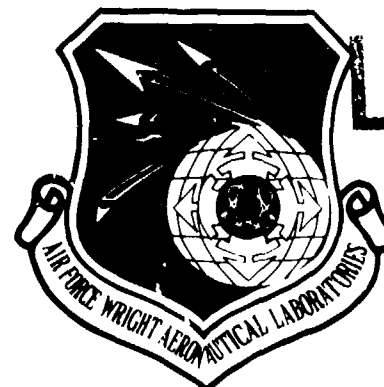


3

AFWAL-TR-81-3103



LEVEL II

AD A108987

FLUTTER AND TIME RESPONSE ANALYSES  
OF THREE DEGREE OF FREEDOM AIRFOILS  
IN TRANSONIC FLOW

T.Y. Yang  
C.H. Chen  
School of Aeronautics and Astronautics  
Purdue University  
West Lafayette, Indiana 47907

August 1981

Final Report for Period November 1979-December 1980

Approved for public release; distribution unlimited.

DTIC FILE COPY

FLIGHT DYNAMICS LABORATORY  
AIR FORCE WRIGHT AERONAUTICAL LABORATORIES  
AIR FORCE SYSTEMS COMMAND  
WRIGHT-PATTERSON AIR FORCE BASE, OHIO 45433

DTIC  
ELECTE  
DEC 30 1981  
S D D

8

01 12 28 475

# NOTICE

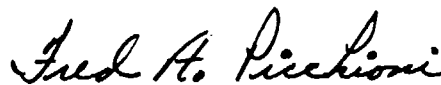
When Government drawings, specifications, or other data are used for any purpose other than in connection with a definitely related Government procurement operation, the United States Government thereby incurs no responsibility nor any obligation whatsoever; and the fact that the government may have formulated, furnished, or in any way supplied the said drawings, specifications, or other data, is not to be regarded by implication or otherwise as in any manner licensing the holder or any other person or corporation, or conveying any rights or permission to manufacture use, or sell any patented invention that may in any way be related thereto.

This report has been reviewed by the Office of Public Affairs (ASD/PA) and is releasable to the National Technical Information Service (NTIS). At NTIS, it will be available to the general public, including foreign nations.

This technical report has been reviewed and is approved for publication.



LAWRENCE J. HUTTSELL  
Aerospace Engineer  
Aeroelastic Group



FREDERICK A. PICCHIONI, Lt Col, USAF  
Chief, Analysis & Optimization Branch  
Structures & Dynamics Division

FOR THE COMMANDER



RALPH L. KUSTER, JR., Colonel, USAF  
Chief, Structures & Dynamics Division

"If your address has changed, if you wish to be removed from our mailing list, or if the addressee is no longer employed by your organization please notify AFWAL/FIBRC W-PAFB, OH 45433 to help us maintain a current mailing list."

Copies of this report should not be returned unless return is required by security considerations, contractual obligations, or notice on a specific document.

UNCLASSIFIED

SECURITY CLASSIFICATION OF THIS PAGE (When Data Entered)

REPORT DOCUMENTATION PAGE		READ INSTRUCTIONS BEFORE COMPLETING FORM
1. REPORT NUMBER AFWAL-TR-81-3103	2. GOVT ACCESSION NO. AD-710887	3. RECIPIENT'S CATALOG NUMBER
4. TITLE (and Subtitle) FLUTTER AND TIME RESPONSE ANALYSES OF THREE DEGREE OF FREEDOM AIRFOILS IN TRANSONIC FLOW		5. TYPE OF REPORT & PERIOD COVERED Final Report November 1979-December 1980
		6. PERFORMING ORG. REPORT NUMBER
7. AUTHOR(s)  T.Y. Yang and C.H. Chen		8. CONTRACT OR GRANT NUMBER(s)  AFOSR-78-3523
9. PERFORMING ORGANIZATION NAME AND ADDRESS School of Aeronautics and Astronautics Purdue University West Lafayette, Indiana 47907		10. PROGRAM ELEMENT, PROJECT, TASK AREA & WORK UNIT NUMBERS PE 61102 F 2307/N5/11
11. CONTROLLING OFFICE NAME AND ADDRESS Air Force Wright Aeronautical Laboratories (FIBR) Wright-Patterson AFB, Ohio 45433		12. REPORT DATE August 1981
		13. NUMBER OF PAGES 61
14. MONITORING AGENCY NAME & ADDRESS (if different from Controlling Office)		15. SECURITY CLASS. (of this report) Unclassified
		15a. DECLASSIFICATION/DOWNGRADING SCHEDULE
16. DISTRIBUTION STATEMENT (of this Report)  Approved for public release; distribution unlimited.		
17. DISTRIBUTION STATEMENT (of the abstract entered in Block 20, if different from Report)		
18. SUPPLEMENTARY NOTES		
19. KEY WORDS (Continue on reverse side if necessary and identify by block number) Airfoils Flutter Supercritical Transonic Unsteady Aerodynamics		
20. ABSTRACT (Continue on reverse side if necessary and identify by block number) Flutter and time response analyses are performed for a NACA 64A006 conventional and a MBB A-3 supercritical airfoil, both oscillating with plunge, pitch, and aileron pitch d.o.f.'s in small disturbance, transonic flow. The aerodynamic coefficients are calculated using the transonic code LTRAN2-NLR. The effects of various kinds of aeroelastic parameters on flutter speeds for the bending-torsion, bending-aileron, and torsion-aileron branches are studied. The flutter speeds associated with the		

DD FORM 1473

1 JAN 73

EDITION OF 1 NOV 65 IS OBSOLETE

UNCLASSIFIED

SECURITY CLASSIFICATION OF THIS PAGE (When Data Entered)

UNCLASSIFIED

SECURITY CLASSIFICATION OF THIS PAGE(When Data Entered)

bending-torsion branch are plotted against Mach number for different parameter values. The flutter speed, the amplitude ratio, and the phase difference at different Mach numbers are plotted against the mass ratio for both a two d.o.f. and a three d.o.f. case. Time-response results are obtained for the NACA 64A006 and the MBB A-3 airfoils at  $M = 0.85$  and  $0.765$ , respectively. Using the same sets of parameter values, the flight speeds used to obtain all the neutrally stable response are very close to the flutter speeds obtained in the flutter analysis. The principle of linear superposition of airloads is used in the flutter analysis but not in the response analysis.

UNCLASSIFIED

SECURITY CLASSIFICATION OF THIS PAGE(When Data Entered)

## FOREWORD

This report was prepared by Professor T.Y. Yang of the School of Aeronautics and Astronautics of Purdue University under AFOSR Grant 78-3523, "Application of Time-Accurate Transonic Aerodynamics to Aeroelastic Problems." The research grant was administered by Lawrence J. Huttshell of the Structures and Dynamics Division, Flight Dynamics Laboratory, Air Force Wright Aeronautical Laboratories, Wright-Patterson Air Force Base, Ohio.

The report covers work conducted from November 1979 to December 1980. The work was performed by C.H. Chen, a graduate research assistant, in partial fulfillment of his Ph.D. requirements. T.Y. Yang was the principal advisor.

<b>Accession For</b>	
NTIS GRA&I	<input checked="checked" type="checkbox"/>
DTIC TAB	<input type="checkbox"/>
Unannounced	<input type="checkbox"/>
Justification	
By _____	
Distribution/	
Availability Codes	
Dist	Avail and/or Special
A	

## TABLE OF CONTENTS

SECTION	PAGE
I INTRODUCTION .....	1
II FLUTTER EQUATION AND SOLUTION PROCEDURE.....	5
III EQUATIONS OF MOTION AND RESPONSE ANALYSIS PROCEDURE.....	9
IV RESULTS OF AERODYNAMIC COMPUTATIONS.....	11
V RESULTS OF FLUTTER ANALYSIS.....	23
1. Effect of Frequency Ratios ( $\omega_\beta/\omega_\alpha$ and $\omega_h/\omega_\alpha$ ).....	23
2. Effect of Mass Ratio ( $\mu$ ).....	25
3. Effect of the Position of Airfoil Mass Center ( $x_\alpha$ ).....	27
4. Effect of the Position of Elastic Axis ( $a_h$ ) .....	29
5. Effect of the Position of Aileron Mass Center ( $x_\beta$ ).....	29
6. Effect of Mach Number (M) .....	32
7. Discussion of the Flutter Modes.....	34
VI RESULTS OF TIME RESPONSE ANALYSIS.....	39
VII CONCLUDING REMARKS.....	45
REFERENCES.....	47

PRECEDING PAGE BLANK-NOT FILMED

## LIST OF ILLUSTRATIONS

FIGURE	PAGE
1 Definition of Parameters for Three Degree of Freedom Aerelastic Analysis.....	6
2 Distribution of Steady Pressure Coefficients for NACA 64A006 Airfoil.....	12
3 Distribution of Steady Pressure Coefficients for MBB A-3 Airfoil with $c_x \approx 0.58$ .....	13
4 Effect of Aileron-Airfoil Pitch Frequency on Flutter Speed for Three Different Airfoil Plunge-Pitch Frequency Ratios.....	24
5 Effect of Mass Ratio on Flutter Speed.....	26
6 Effect of Position of Airfoil Mass Center on Flutter Speed.....	28
7 Effect of Position of Elastic Axis on Flutter Speed.....	30
8 Effect of Position of Aileron Mass Center on Flutter Speed.....	31
9 Effect of Mach Number on Flutter Speed for Both Airfoils for Two Mass Ratios: (a) $\mu=20$ and (b) $\mu=50$ .....	33
10 Flutter Speed and Flutter Mode (Amplitude Ratio and Phase Angle) vs. Mass Ratio for Both Airfoils for a Two D.O.F. Case with $a_h=-2$ .....	35
11 Flutter Speed and Flutter Mode (Amplitude Ratio and Phase Angle) vs. Mass Ratio for plunge and pitch, $a_h=-0.2$ .....	37
12 Flutter Speed and Flutter Mode (Amplitude Ratios and Phase Angles) vs. Mass Ratio for the MBB A-3 Airfoil for a Three D.O.F. Case with $a_h=-0.2$ .....	38
13 Effect of Flutter Speed on Displacement Responses for The NACA 64A006 Airfoil at $M = 0.85$ .....	40
14 Effect of Flutter Speed on Aerodynamic Responses for the NACA 64A006 Airfoil at $M = 0.85$ .....	41

## LIST OF ILLUSTRATIONS (Continued)

FIGURE		PAGE
15	Effect of Flutter Speed on Displacement Responses for the MBB A-3 Airfoil at $M=0.765$ .....	42
16	Effect of Flutter Speed on Aerodynamic Responses for the MBB A-3 Airfoil at $M=0.765$ .....	43



# LIST OF TABLES

TABLE		PAGE
1	Aerodynamic Coefficients for the NACA 64A006 Airfoil Pitching at the Quarter Chord at $M=0.7$ .....	15
2	Aerodynamic Coefficients for the NACA 64A006 Airfoil Pitching at the Quarter Chord at $M=0.8$ .....	16
3	Aerodynamic Coefficients for the NACA 64A006 Airfoil Pitching at the Quarter Chord at $M=0.85$ .....	17
4	Aerodynamic Coefficients for the NACA 64A006 Airfoil Pitching at the Quarter Chord at $M=0.875$ .....	18
5	Aerodynamic Coefficients for the MBB A-3 Airfoil at $M=0.7$ and $\alpha=1.2^\circ$ .....	19
6	Aerodynamic Coefficients for the MBB A-3 Airfoil at $M=0.74$ and $\alpha=1.2^\circ$ .....	20
7	Aerodynamic Coefficients for the MBB A-3 Airfoil at $M=0.765$ and $\alpha=0.86^\circ$ .....	21
8	Aerodynamic Coefficients for the MBB A-3 Airfoil at $M=0.78$ and $\alpha=0.6^\circ$ .....	22

# NOMENCLATURE

$a_h$	- distance in semi-chord measured from mid-chord to elastic axis
$[A]$	- matrix of aerodynamic coefficients
$b, c$	- semi-chord and full-chord, respectively
$c_p^*$	- critical pressure coefficient
$c_\ell$	- lift coefficient
$c_m$	- moment coefficient about pitching axis
$c_n$	- moment coefficient about aileron hinge axis
$c_\beta$	- distance in semi-chord measured from mid-chord to aileron hinge axis
$dc_\ell$	- differential $c_\ell$ relative to the mean value of $c_\ell$ in forced motion
$dc_m$	- differential $c_m$ relative to the mean value of $c_m$ in forced motion
$dc_n$	- differential $c_n$ relative to the mean value of $c_n$ in forced motion
$g$	- structural damping coefficient
$h$	- plunging degree of freedom
$I_\alpha$	- polar moment of inertia about elastic axis
$I_\beta$	- polar moment of inertia about aileron hinge axis
$k_c$	- $\omega c/U$ , reduced frequency with respect to full chord
$[K]$	- matrix of stiffness coefficients
$\{p\}$	- aerodynamic load vector
$\{q\}$	- displacement vector
$r_\alpha$	- $(I_\alpha/mb^2)^{1/2}$ , radius of gyration about elastic axis
$r_\beta$	- $(I_\beta/mb^2)^{1/2}$ , radius of gyration of aileron about aileron hinge axis
$S_\alpha$	- airfoil static moment about elastic axis
$S_\beta$	- aileron static moment about aileron hinge axis
$t$	- time in seconds
$\bar{t}$	- $\omega t$ , nondimensional time

- $U$  - free stream velocity
- $U^*$  -  $U/b\omega_\alpha$ , nondimensional flight speed
- $x_\alpha$  -  $S_\alpha/mb$ , distance in semi-chord measured from elastic axis to mass center
- $x_\beta$  -  $S_\beta/mb$ , distance in semi-chord measured from aileron hinge axis to aileron mass center
- $\alpha$  - pitching degree of freedom
- $\beta$  - aileron pitching degree of freedom
- $\delta$  -  $h/c$ , nondimensional plunging degree of freedom
- $\phi_{h,\alpha}$  - phase difference between plunging and pitching oscillation, plunging leading the pitching
- $\phi_{h,\beta}$  - phase difference between plunging and aileron pitching oscillation, plunging leading the pitching
- $\mu$  -  $m/\pi\rho b^2$ , mass ratio
- $\omega$  - flutter frequency
- $\omega_h$  -  $(K_h/m)^{1/2}$ , uncoupled plunging natural frequency
- $\omega_\alpha$  -  $(K_\alpha/I_\alpha)^{1/2}$ , uncoupled pitching natural frequency of airfoil about elastic axis
- $\omega_\beta$  -  $(K_\beta/I_\beta)^{1/2}$ , uncoupled pitching natural frequency of aileron about elastic axis
- $\omega_r$  - reference frequency
- $\rho$  - free stream air density
- $\xi$  -  $h/b$ , nondimensional plunging degree of freedom

#### Subscripts

- $o$  - absolute amplitude of displacement
- $\delta$  - due to plunging degree of freedom  $\delta$
- $\alpha$  - due to pitching degree of freedom  $\alpha$
- $\beta$  - due to aileron pitching degree of freedom  $\beta$

## SECTION I

### INTRODUCTION

The numerical methods and computer codes for transonic unsteady aerodynamics have been developed significantly in recent years. A state-of-the-art review of the numerical methods was given by Ballhaus and Bridgeman (Reference 1). Aeroelastic applications of these developments were performed and reviewed by many authors, such as Ashley (Reference 2), Mykytow (Reference 3), Yang, Guruswamy, and Striz (Reference 4).

Farmer and Hanson (Reference 5) performed an experimental flutter analysis of two dynamically similar wings, one with supercritical sections and the other with conventional sections. It was found that the experimental results agreed with those calculated from the subsonic lifting surface theory up to the Mach number of 0.85. Beyond that Mach number, the experimental curves for dynamic pressure showed a transonic dip and the supercritical wing experienced a much more pronounced transonic dip.

Flutter analyses of airfoils oscillating with only two d.o.f.'s (plunge and pitch) were carried out extensively. Rizzetta (Reference 6) used STRANS2 and UTRANS2 (Reference 7) to analyze a NACA 64A010 airfoil. Yang, Striz, and Guruswamy used STRANS2, UTRANS2, and LTRAN2 (Reference 8) to analyze a NACA 64A006 (Reference 9), a MBB A-3 (Reference 10), and a NACA 64A010 (Reference 4) airfoil. They also used STRANS2 and UTRANS2 to analyze a TF-8A wing section (Reference 4). In the analysis of the streamwise section of a sweptback wing, Isogai (Reference 11) concluded that the mechanism of the single d.o.f. flutter dominates the flutter of the system studied at the bottom of the transonic dip.

Isogai (Reference 12) also developed a transonic small-perturbation code which can be used for the reduced frequency  $k_c$  with values up to 1.0 and the entire Mach number range. He used the code to study the NACA 64A010 airfoil for two cases, simulating characteristics of a streamwise section of a sweptback and an unswept wing, respectively.

McGrew et al. (Reference 13) carried out flutter analysis of a TF-8A flutter model. It was demonstrated that supercritical wings exhibited significantly lower flutter speeds than a conventional wing of equal size and rigidities.

Eastep and Olsen (Reference 14) reported the flutter analysis of a rectangular wing by using the 3-D unsteady transonic codes TDSTRN and TDUTRN (Reference 7).

In addition to the flutter analysis, aeroelastic time-response analysis has also become a topic of recent interest. Ballhaus and Goorjian (Reference 15) first performed a time-response analysis of a NACA 64A006 airfoil oscillating with single pitch d.o.f. at  $M = 0.88$ . The time-response analysis was computed by using their program LTRAN2 for unsteady flow coupled with an integration procedure for the structural equation of motion.

Rizzetta (Reference 16) performed a time-response analysis of a NACA 64A010 airfoil with a single pitch d.o.f. and three d.o.f.'s - pitch, plunge, and aileron pitch. The LTRAN2 code was used. It was pointed out in Reference 16 that no attempt was made to obtain the neutrally stable response curves corresponding to the flutter condition for the three d.o.f. system.

Guruswamy and Yang (Reference 17) performed a time-response analysis of a NACA 64A006 airfoil oscillating with plunge and pitch d.o.f.'s at

M = 0.7 and 0.85, respectively. Again, LTRAN2 was used. Parameters that resulted in the neutrally stable response agreed with those equivalent to the flutter conditions found in the separate flutter analysis. The principle of linear superposition of airloads was used in the flutter analysis but not in the response analysis.

Recently, several modifications have been incorporated into LTRAN2. Houwink and van der Vooren (Reference 18) improved the LTRAN2 code by developing the NLR (National Aerospace Laboratory of the Netherlands) version. High-frequency terms were added to the boundary conditions and the pressure computations. Rizzetta and Chen (Reference 19) and Rizzetta and Yoshihara (Reference 20) included the  $\phi_{tt}$  term in the small-disturbance equation. There is no longer the assumption of low reduced-frequency. Viscous effects were incorporated in the code by using a viscous ramp method (Reference 20).

Goorjian (Reference 21) gave a preliminary study to remove the small-disturbance and low-frequency restrictions by considering the full potential equation. Borland, Rizzetta, and Yoshihara (Reference 22) developed a transonic code LTRAN3 which can solve the 3-D low-frequency, unsteady transonic equation by the time-integration method.

Among these new developments, the LTRAN2-NLR appears to be an attractive code for aeroelastic applications. In the computation of the unsteady aerodynamic coefficients, the LTRAN2-NLR can lift the limit of the reduced frequency (in full chord) from, say, 0.2 or 0.3 for LTRAN2 to at least 0.8. With this new capability, the flutter analysis and the time-response predictions for the three d.o.f. (plunge, pitch, and aileron pitch) systems become more feasible. More realistic and broader ranges of parameter values can be considered.

In this study, LTRAN2-NLR is used to analyze a NACA 64A006 conventional and a MBB A-3 supercritical airfoil fitted with trailing edge ailerons at 25% of the chord. Three d.o.f.'s are considered. Flutter analysis is first performed and the effects of various parameters are studied. The neutrally stable time-response predictions are then obtained. The effect of the mass ratio on the flutter modes (amplitude ratios and phase differences) for various Mach numbers are studied.

## SECTION II

### FLUTTER EQUATION AND SOLUTION PROCEDURE

The parameters and sign conventions for the airfoil with pitch, plunge, and aileron pitch d.o.f.'s are defined in Figure 1. The system is similar to that discussed in Sec. 6.10 of Reference 23.

Based on the derivations given in Reference 23, the flutter equation can be written in the form as,

$$\left[ \frac{1}{4} \mu k_c^2 [M] - \frac{1}{\pi} [A] \right] \begin{Bmatrix} \xi \\ \alpha \\ \beta \end{Bmatrix} = \lambda [K] \begin{Bmatrix} \xi \\ \alpha \\ \beta \end{Bmatrix} \quad (1)$$

where  $\mu = m/\pi \rho b^2$  is the mass ratio;  $k_c = \omega c/U$  is the reduced frequency;  $\xi = h/b$  is the nondimensional plunge displacement; the three matrices are defined as

$$[M] = \begin{bmatrix} 1 & x_\alpha & x_\beta \\ x_\alpha & r_\alpha^2 & (c_\beta - a_h)x_\beta + r_\beta^2 \\ x_\beta & (c_\beta - a_h)x_\beta + r_\beta^2 & r_\beta^2 \end{bmatrix} \quad (2a)$$

$$[A] = \begin{bmatrix} \frac{1}{2} c_{l\delta} & c_{l\alpha} & c_{l\beta} \\ -c_{m\delta} & -2c_{m\alpha} & -2c_{m\beta} \\ -c_{n\delta} & -2c_{n\alpha} & -2c_{n\beta} \end{bmatrix} \quad (2b)$$



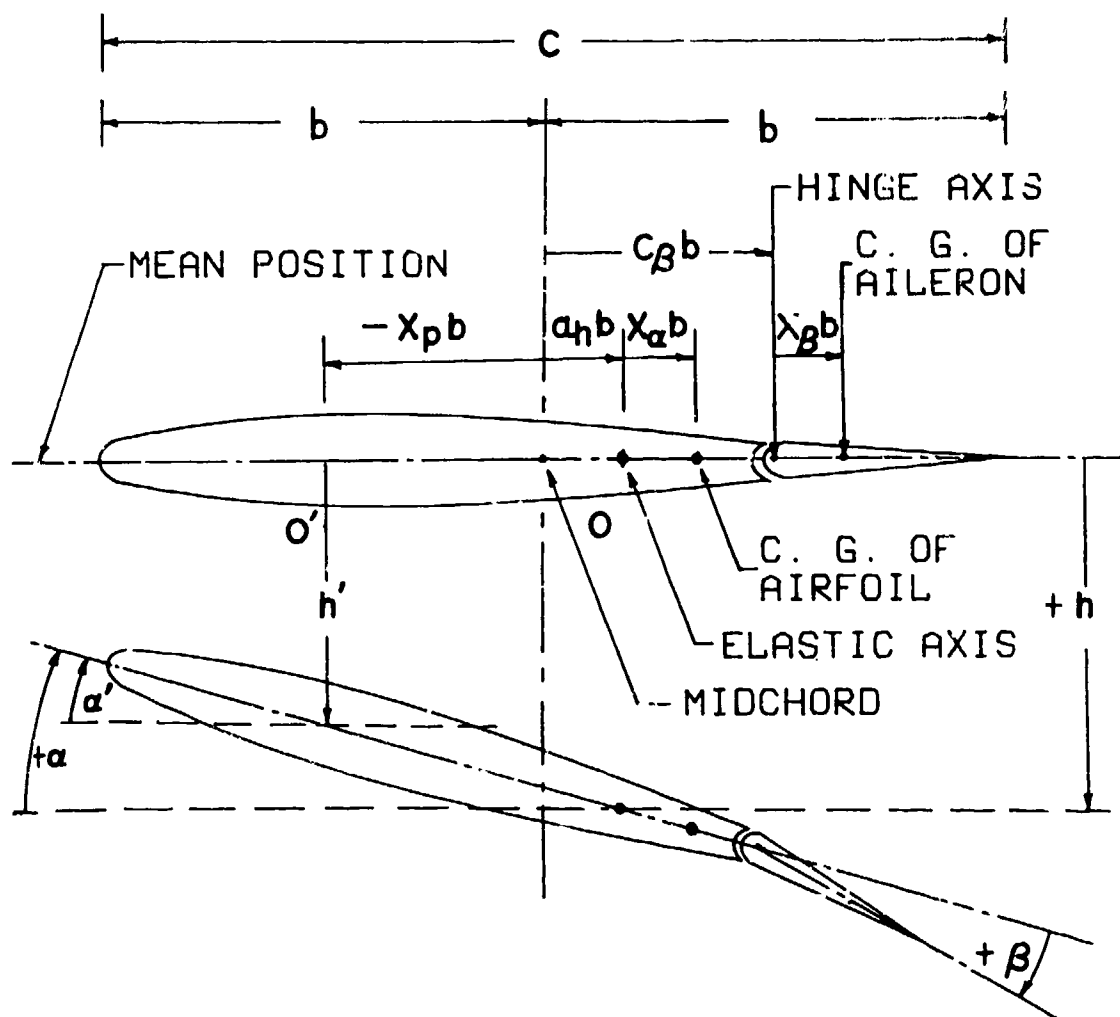


Figure 1 Definition of Parameters for Three Degree of Freedom Aeroelastic Analysis

$$[K] = \begin{bmatrix} (\omega_h/\omega_r)^2 & 0 & 0 \\ 0 & r_\alpha^2 (\omega_\alpha/\omega_r)^2 & 0 \\ 0 & 0 & r_\beta^2 (\omega_\beta/\omega_r)^2 \end{bmatrix} \quad (2c)$$

where  $r_\alpha = (I_\alpha/m b^2)^{1/2}$  and  $r_\beta = (I_\beta/m b^2)^{1/2}$  are the radii of gyration of the airfoil and aileron about the elastic axis and the aileron hinge axis, respectively; matrix  $[A]$  contains the 9 aerodynamic coefficients associated with the three respective d.o.f.'s;  $\omega_h = (K_h/m)^{1/2}$ ,  $\omega_\alpha = (K_\alpha/I_\alpha)^{1/2}$ ,  $\omega_\beta = (K_\beta/I_\beta)^{1/2}$  are the three uncoupled natural frequencies; and  $\omega_r = \omega_\alpha$  is the reference frequency.

The eigenvalue  $\lambda$  is a complex number defined as

$$\lambda = \mu (1 + ig) \omega_r^2 b^2/U^2 \quad (2)$$

where  $g$  is the so-called structural damping coefficient. The flutter solution is obtained when  $g$  is found to be zero (Reference 23). The flutter speed is nondimensionalized as

$$U^* = U/b\omega_\alpha = (\omega_r/\omega_\alpha) \sqrt{\mu/\lambda}$$

In the present flutter analysis, the principle of linear superposition of airloads was assumed valid in deriving the flutter equation.

Justification of this principle was studied experimentally by Davis and Malcolm (Reference 24) for a NACA 64A010 airfoil oscillating with plunge and pitch d.o.f.'s. In the conclusion, they stated that the principles of superposition and linearity were shown to be valid for supercritical attached flow. In a time-response analysis of a

NACA 64A006 airfoil oscillating with plunge and pitch d.o.f.'s, Guruswamy and Yang (Reference 17) showed in a specific example that the parameter values associated with the flutter speed at the bottom of a transonic dip can indeed be used to obtain the neutrally stable response. The principle of superposition was used in the flutter analysis but not in the response analysis.

As an attempt to validate this principle in its application to flutter analysis of three d.o.f. case, neutrally stable response results are obtained for three specific examples where alternative flutter solutions are found in the flutter analysis.

In the flutter analysis, the elastic axis does not always coincide with the pitching axis for which the aerodynamic data are obtained.

The equations for transforming the aerodynamic coefficients for a pitching axis  $O'$  (see Figure 1) to those for another pitching axis (elastic axis)  $O$  are in the following form (Reference 7)

$$\begin{cases} c_{l\delta} = c_{l\delta}' \\ c_{l\alpha} = c_{l\alpha}' - s c_{l\delta}' \\ c_{l\beta} = c_{l\beta}' \end{cases} \quad \begin{cases} c_{n\delta} = c_{n\delta}' \\ c_{n\alpha} = c_{n\alpha}' - s c_{n\delta}' \\ c_{n\beta} = c_{n\beta}' \end{cases}$$

$$\begin{cases} c_{m\delta} = c_{m\delta}' + s c_{l\delta}' \\ c_{m\alpha} = c_{m\alpha}' + s(c_{l\alpha}' - c_{m\delta}') - s^2 c_{r\delta}' \\ c_{m\beta} = c_{m\beta}' + s c_{l\beta}' \end{cases} \quad (3)$$

where  $s = (a_h - x_p)/2$

### SECTION III

#### EQUATIONS OF MOTION AND RESPONSE ANALYSIS PROCEDURE

The time-response analysis is based on the following equations of motion

$$[M] \begin{Bmatrix} \xi'' \\ \alpha'' \\ \beta'' \end{Bmatrix} + \left( \frac{2 \omega_r}{U^* k_c \omega_\alpha} \right)^2 [K] \begin{Bmatrix} \xi \\ \alpha \\ \beta \end{Bmatrix} = \left( \frac{4}{\pi \mu k_c^2} \right) \begin{Bmatrix} -c_\ell \\ 2c_m \\ 2c_n \end{Bmatrix} \quad (4)$$

where the prime indicates derivative with respect to nondimensional time  $\bar{t} = \omega t$ .

Equation 4 can be written in a simplified symbolic form as

$$[M] \{q''\} + [N] \{q\} = \{P\} \quad (5)$$

where  $\{q\}$  is the vector for the three d.o.f.'s;  $[N] = (2\omega_r/U^* k_c \omega_\alpha)^2 [K]$ ; and  $\{P\}$  is the vector of aerodynamic forces. This equation can be solved by a step-by-step time-integration finite difference approach.

Assuming a linear variation of acceleration, the velocities and displacements after a small time step  $\Delta t$  can be expressed as

$$\begin{aligned} \{q'\}_{\bar{t}} &= \{q'\}_{\bar{t}-\Delta\bar{t}} + \frac{\Delta\bar{t}}{2} \{q''\}_{\bar{t}-\Delta\bar{t}} + \frac{\Delta\bar{t}}{2} \{q''\}_{\bar{t}} \\ \{q\}_{\bar{t}} &= \{q\}_{\bar{t}-\Delta\bar{t}} + \Delta\bar{t} \{q'\}_{\bar{t}-\Delta\bar{t}} + \frac{\Delta\bar{t}^2}{3} \{q''\}_{\bar{t}-\Delta\bar{t}} + \frac{\Delta\bar{t}^2}{6} \{q''\}_{\bar{t}} \end{aligned} \quad (6)$$

Substituting Equations 6 into Equation 5 yields

$$\{q''\}_{\bar{t}} = [F] \left[ \{p\}_{\bar{t}} - [N] \{r\} \right] \quad (7)$$

where

$$[F] = \left[ [M] + \frac{\Delta \bar{t}^2}{6} [N] \right]^{-1} \quad (8a)$$

$$\{r\} = \{q\}_{\bar{t}-\Delta \bar{t}} + \Delta \bar{t} \{q'\}_{\bar{t}-\Delta \bar{t}} + \frac{\Delta \bar{t}^2}{3} \{q''\}_{\bar{t}-\Delta \bar{t}} \quad (8b)$$

This direct integration method for structural response analysis is well-known (Reference 25). In this study, the vector for aerodynamic forces is obtained using the LTRAN2-NLR code.

In each time step,  $\{q''\}$  at the time  $\bar{t}$  are first obtained from the known values of  $\{q\}$ ,  $\{q'\}$ , and  $\{p\}$  at  $\bar{t}-\Delta \bar{t}$  from Equation 6. Based on the known values of  $\{q\}$  and  $\{q'\}$ , the aerodynamic force vector  $\{p\}$  at the time  $\bar{t}$  can be obtained using LTRAN2-NLR code. A detailed description of the time-response analysis procedure is given in Reference 17.

In order to obtain the neutrally stable responses for flutter condition earlier, the aerodynamic equation alone may be integrated in time for several cycles in response to the forced motion. The displacement vector of the airfoil is specified according to the amplitude ratios and the phase angles of the flutter mode of the three d.o.f. system. After the aerodynamic responses become periodic, the system is set free, the simultaneous integration procedure begins, and the airfoil and the aerodynamic forces drive each other.

## SECTION IV

### RESULTS OF AERODYNAMIC COMPUTATIONS

A NACA 64A006 conventional and a MBB A-3 supercritical airfoil were studied. Both configurations were among those proposed by AGARD for aeroelastic applications of transonic unsteady aerodynamics. The airfoil coordinates used (Reference 26) are somewhat different from the values used in previous applications. Both the steady and unsteady aerodynamic coefficients were computed by using LTRAN2-NLR code (Reference 18).

Figure 2 shows the steady pressure distributions for the NACA 64A006 airfoil with zero angle of attack for  $M = 0.7, 0.8, 0.85$ , and  $0.875$ . The experimental results obtained by Tijdeman (Reference 27) at  $M = 0.85$  are also plotted. At  $M = 0.85$ , a weak shock wave exists and the present results agree well with those by Tijdeman except in the neighborhood of 30~40% of the chord. At  $M = 0.875$ , a strong shock wave is formed.

The design conditions for the MBB A-3 airfoil are:  $M = 0.765$ ;  $c_{\lambda} = 0.58$ ,  $\alpha = 1.3^{\circ}$ . In an attempt to match the design lift coefficient of 0.58, the angles of attack were chosen as  $1.2^{\circ}, 1.2^{\circ}, 0.86^{\circ}$ , and  $0.6^{\circ}$  for Mach numbers 0.7, 0.74, 0.765, and 0.78, respectively. The steady pressure distributions for the four cases were plotted in Figure 3. Also plotted are the experimental results of Bucciantini, Oggiano, and Onorato (Reference 28) obtained in Bedford Wind Tunnel for  $M = 0.765$ ,  $c_{\lambda} = 0.519$ , and  $\alpha = 1.5^{\circ}$ . For  $M = 0.765$ , a very weak shock wave occurs in the neighborhood of 55~65% of the chord. The results agree well with the experimental data except in the neighborhood of 40~60% of the chord. The present angle of attack is, however, smaller than that used in Reference 28. For  $M = 0.78$ , the shock wave becomes stronger and shifts aft.

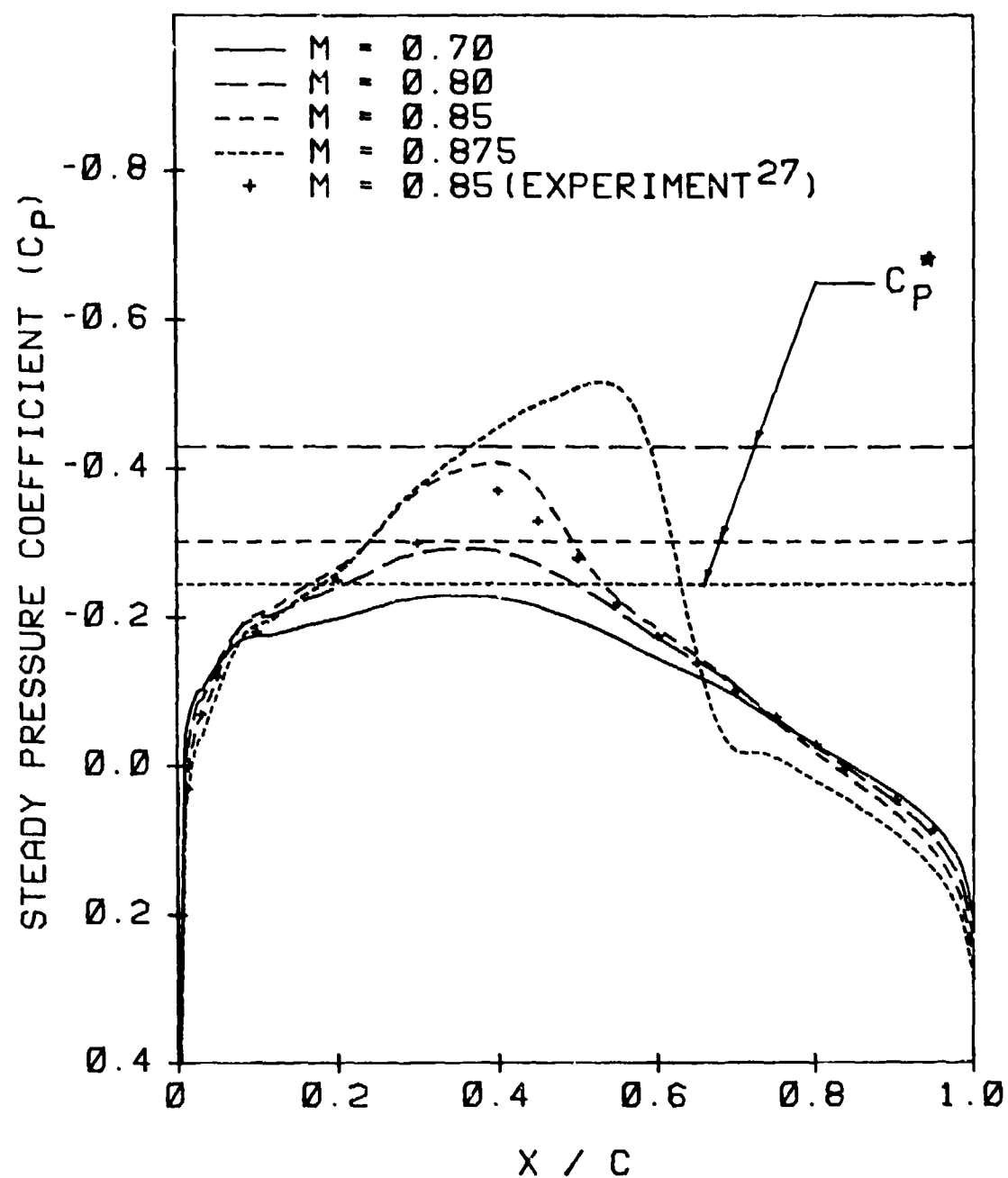


Figure 2 Distribution of Steady Pressure Coefficients  
for NACA 64A006 Airfoil

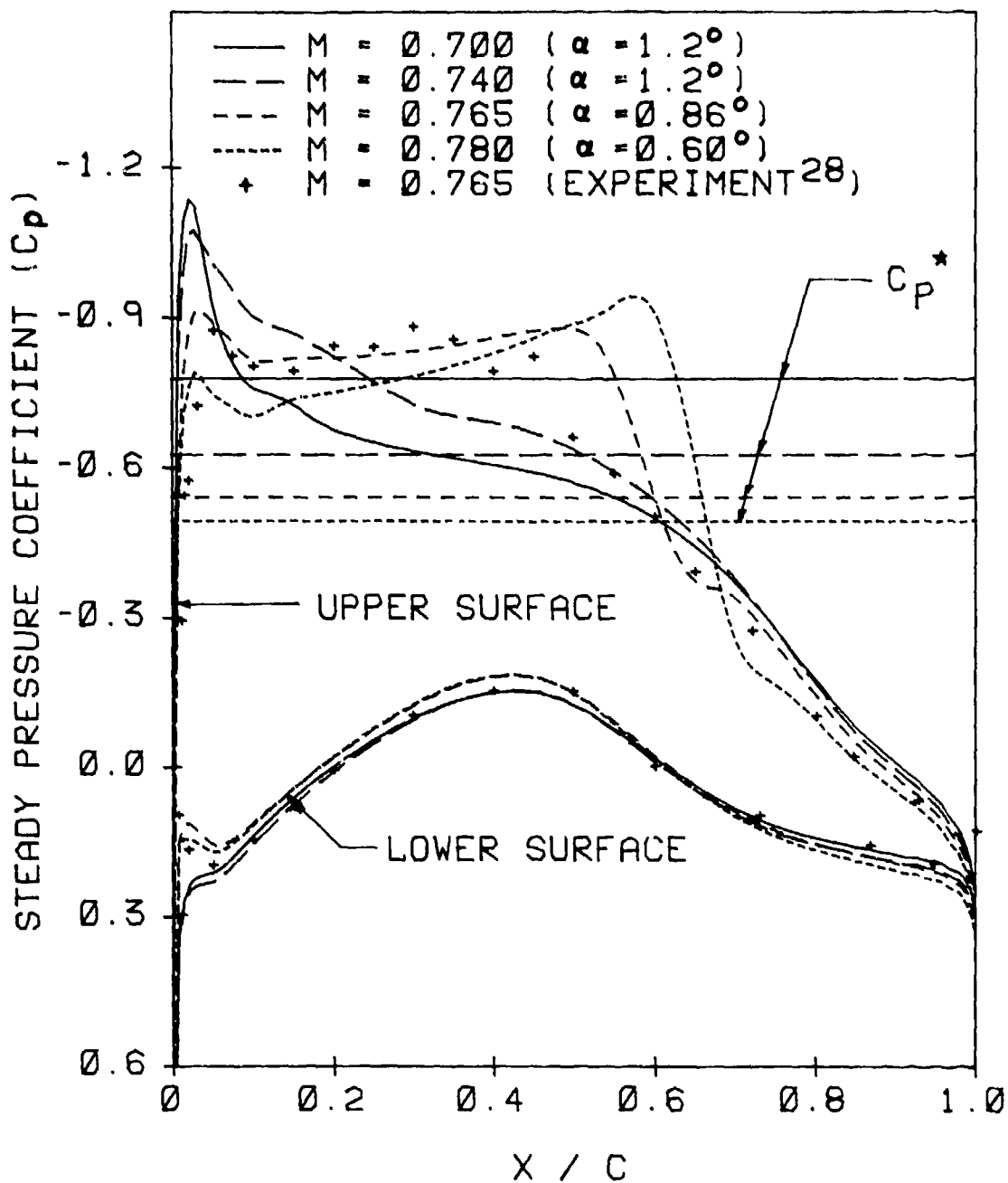


Figure 3 Distribution of Steady Pressure Coefficients for MBB A-3 Airfoil with  $c_{\ell} = 0.58$



In the unsteady aerodynamic calculations, 60 time steps were used for each half-cycle. The amplitudes chosen were  $0.1C$  and  $0.1^\circ$  for the plunge and pitch d.o.f.'s, respectively. The nine aerodynamic coefficients  $c_{l\delta}$ ,  $c_{l\alpha}$ ,  $c_{l\beta}$ ,  $c_{m\delta}$ ,  $c_{m\alpha}$ ,  $c_{m\beta}$ ,  $c_{n\delta}$ ,  $c_{n\alpha}$ , and  $c_{n\beta}$  were computed by using a  $79 \times 99$  grid. Both airfoils fitted with trailing edge ailerons of 25% chord, were assumed to pitch about the quarter chord axis. The results were given in Tables 1 to 8 with reduced frequency  $k_c$  equal to 0.1, 0.2, 0.3, 0.4, 0.6, 0.8, 1.2, and 1.6 for each Mach number considered.

Table 1. Aerodynamic Coefficients for the NACA 64A006

Airfoil Pitching at the Quarter Chord at  $M=0.7$

$k_c$	$C_{L\delta}$		$C_{L\alpha}$		$C_{L\beta}$		$C_{m\delta}$		$C_{m\alpha}$	
	Real	Imag	Real	Imag	Real	Imag	Real	Imag	Real	Imag
.05	.066	0.41	8.28	-1.31	5.14	-0.82	.005	-.010	-.205	-.091
0.1	.161	0.76	7.55	-1.61	4.62	-1.24	.015	-.019	-.189	-.153
0.2	.385	1.24	6.44	-1.73	3.92	-1.28	.028	-.042	-.166	-.287
0.3	.508	1.65	5.91	-.940	3.43	-1.32	.061	-.063	-.160	-.416
0.4	.557	2.02	5.54	-.290	3.14	-1.21	.108	-.085	-.148	-.553
0.5	.520	2.46	5.28	0.012	2.93	-1.12	.176	-.108	-.146	-.686
0.6	.491	2.73	5.12	0.538	2.77	-1.06	.245	-.135	-.130	-.822
0.8	.255	3.47	4.95	1.327	2.60	-0.84	.427	-.203	-.058	-1.11
1.2	-.77	5.03	4.92	3.140	2.41	-0.60	1.03	-.365	-.110	-1.69
1.6	-1.9	7.06	5.27	4.530	2.24	-0.52	1.79	-.715	-.178	-2.37

$k_c$	$C_{m\beta}$		$C_{n\epsilon}$		$C_{n\alpha}$		$C_{n\beta}$	
	Real	Imag	Real	Imag	Real	Imag	Real	Imag
.05	-1.04	-0.027	0.0001	-.0025	-.0502	-.0005	-.0879	-.0018
0.1	-1.03	-0.036	0.0002	-.0047	-.0467	-.0025	-.0856	-.0019
0.2	-1.03	-0.063	0.0005	-.0084	-.0416	-.0135	-.0831	-.0059
0.3	-1.03	-0.088	0.0023	-.0118	-.0376	-.0244	-.0813	-.0114
0.4	-1.04	-0.114	0.0053	-.0151	-.0346	-.0346	-.0806	-.0171
0.5	-1.06	-0.137	0.0093	-.0187	-.0323	-.0445	-.0805	-.0218
0.6	-1.07	-0.160	0.0148	-.0215	-.0312	-.0539	-.0806	-.0272
0.8	-1.09	-0.196	0.0280	-.0280	-.0205	-.0764	-.0809	-.0364
1.2	-1.16	-0.252	0.0720	-.0400	-.0045	-.1210	-.0829	-.0568
1.6	-1.21	-0.269	0.1350	-.0550	0.0146	-.1710	-.0860	-.0748

Table 2. Aerodynamic Coefficients for the NACA 64A006

Airfoil Pitching at the Quarter Chord at  $M=0.8$

$k_c$	$C_{L\delta}$		$C_{L\alpha}$		$C_{L\beta}$		$C_{m\delta}$		$C_{m\alpha}$	
	Real	Imag	Real	Imag	Real	Imag	Real	Imag	Real	Imag
.05	.106	0.50	10.0	-2.13	6.12	-1.64	.006	-.013	-.253	-.129
0.1	.278	0.86	8.57	-2.78	5.20	-1.99	.020	-.025	-.252	-.204
0.2	.565	1.33	7.02	-2.28	4.04	-2.06	.037	-.061	-.251	-.386
0.3	.750	1.70	6.23	-1.67	3.39	-1.96	.075	-.095	-.281	-.552
0.4	.818	2.08	5.84	-.925	3.02	-1.75	.143	-.134	-.318	-.713
0.5	.810	2.42	5.57	-.585	2.75	-1.59	.210	-.190	-.344	-.896
0.6	.803	2.76	5.41	-.094	2.48	-1.55	.312	-.256	-.416	-1.09
0.8	.707	3.50	5.36	0.563	2.10	-1.37	.523	-.419	-.548	-1.43
1.2	.417	4.98	5.10	1.590	1.47	-0.85	.857	-.952	-.968	-1.79
1.6	-.45	6.28	4.76	2.560	1.39	-0.26	1.18	-1.36	-1.07	-1.91

$k_c$	$C_{m\beta}$		$C_{n\delta}$		$C_{n\alpha}$		$C_{n\beta}$	
	Real	Imag	Real	Imag	Real	Imag	Real	Imag
.05	-1.28	-0.019	0.0000	-.0025	-.0505	-.0001	-.0960	-.0004
0.1	-1.28	-0.032	0.0002	-.0046	-.0462	-.0024	-.0933	-.0023
0.2	-1.30	-0.044	0.0010	-.0084	-.0415	-.0159	-.0915	-.0085
0.3	-1.33	-0.047	0.0045	-.0115	-.0376	-.0305	-.0911	-.0152
0.4	-1.36	-0.039	0.0078	-.0155	-.0347	-.0429	-.0920	-.0220
0.5	-1.39	-0.019	0.0130	-.0190	-.0352	-.0542	-.0935	-.0270
0.6	-1.41	0.0170	0.0193	-.0239	-.0306	-.0688	-.0950	-.0318
0.8	-1.42	0.1160	0.0369	-.0325	-.0259	-.0966	-.0976	-.0415
1.2	-1.19	0.2910	0.0842	-.0572	-.0237	-.1510	-.1026	-.0539
1.6	-0.93	0.1450	0.1450	-.0872	-.0165	-.1010	-.1014	-.0688

Table 3. Aerodynamic Coefficients for the NACA 64A006

Airfoil Pitching at the Quarter Chord at M=0.85

$k_c$	$C_{L\delta}$		$C_{L\alpha}$		$C_{L\beta}$		$C_{m\delta}$		$C_{m\alpha}$	
	Real	Imag	Real	Imag	Real	Imag	Real	Imag	Real	Imag
.05	.210	0.61	12.2	-4.20	7.41	-2.85	.006	-.026	-.510	-.118
0.1	.432	0.97	9.72	-4.33	5.65	-3.26	.026	-.051	-.505	-.257
0.2	.843	1.37	7.40	-3.45	3.85	-3.00	.032	-.129	-.584	-.482
0.3	1.05	1.65	6.34	-2.69	2.85	-2.66	.053	-.210	-.714	-.666
0.4	1.22	1.90	5.86	-2.13	2.28	-2.28	.085	-.316	-.888	-.772
0.5	1.22	2.18	5.32	-1.63	1.82	-1.82	.081	-.382	-.995	-.778
0.6	1.22	2.39	4.84	-1.12	1.66	-1.34	.073	-.459	-1.01	-.707
0.8	.974	2.96	4.48	0.003	1.68	-0.86	.165	-.517	-.876	-.846
1.2	.305	4.41	4.57	1.364	1.72	-0.65	.570	-.790	-.966	-1.31
1.6	-.49	5.92	4.58	2.865	1.58	-0.43	1.04	-1.22	-.939	-1.72

$k_c$	$C_{m\beta}$		$C_{n\delta}$		$C_{n\alpha}$		$C_{n\beta}$	
	Real	Imag	Real	Imag	Real	Imag	Real	Imag
.05	-1.66	0.0300	0.0002	-.0019	-.0375	-.0039	-.1000	-.0035
0.1	-1.67	0.0300	0.0012	-.0035	-.0351	-.0121	-.0938	-.0082
0.2	-1.72	0.0900	0.0032	-.0072	-.0340	-.0275	-.0944	-.0184
0.3	-1.76	0.2470	0.0075	-.0115	-.0332	-.0425	-.0997	-.0249
0.4	-1.70	0.4560	0.0135	-.0165	-.0341	-.0590	-.1060	-.0304
0.5	-1.51	0.5810	0.0190	-.0230	-.0360	-.0740	-.1110	-.0317
0.6	-1.26	0.5870	0.0245	-.0306	-.0410	-.0840	-.1120	-.0300
0.8	-1.04	0.3450	0.0386	-.0430	-.0400	-.1040	-.1080	-.0350
1.2	-.974	0.1660	0.0845	-.0670	-.0344	-.1541	-.1100	-.0520
1.6	-.961	0.0974	0.1460	-.1020	-.0230	-.2060	-.1130	-.0670

Table 4. Aerodynamic Coefficients for the NACA 64A006

Airfoil Pitching at the Quarter Chord at M=0.875

$k_c$	$C_{L\delta}$		$C_{L\alpha}$		$C_{L\beta}$		$C_{m\delta}$		$C_{m\alpha}$	
	Real	Imag	Real	Imag	Real	Imag	Real	Imag	Real	Imag
.05	.666	0.69	14.0	-12.7	7.91	-8.37	-.15	-.143	-2.89	2.733
0.1	.954	0.81	8.25	-8.72	4.41	-6.07	-.21	-.157	-1.64	1.874
0.2	1.14	1.03	5.78	-5.33	2.36	-3.64	-.26	-.167	-1.03	1.089
0.3	1.18	1.27	4.93	-3.55	1.83	-2.39	-.26	-.169	-.842	0.619
0.4	1.16	1.53	4.47	-2.35	1.75	-1.64	-.23	-.169	-.699	0.288
0.5	1.11	1.86	4.36	-1.55	1.75	-1.29	-.16	-.191	-.607	0.014
0.6	1.07	2.21	4.36	-0.55	1.81	-1.09	-.08	-.243	-.605	-.252
0.8	.880	2.87	4.40	0.057	1.75	-0.92	.113	-.367	-.688	-.653
1.2	.350	4.18	4.25	1.203	1.58	-0.54	.490	-.736	-.848	-1.15
1.6	-.40	5.61	4.27	2.177	1.52	-0.34	.925	-1.15	-.905	-1.54

$k_c$	$C_{m\beta}$		$C_{n\delta}$		$C_{n\alpha}$		$C_{n\beta}$	
	Real	Imag	Real	Imag	Real	Imag	Real	Imag
.05	-3.11	2.0800	0.0068	0.0031	0.0581	-.1270	-.0339	-.0904
0.1	-2.27	1.6330	0.0105	-.0002	0.0012	-.1089	-.0739	-.0791
0.2	-1.62	1.2490	0.0148	-.0136	-.0304	-.0940	-.1090	-.0602
0.3	-1.26	1.0200	0.0174	-.0173	-.0461	-.0877	-.1220	-.0450
0.4	-1.06	0.7910	0.0199	-.0250	-.0500	-.0848	-.1238	-.0335
0.5	-.968	0.5930	0.0236	-.0313	-.0535	-.0882	-.1209	-.0284
0.6	-.957	0.4470	0.0294	-.0373	-.0516	-.0963	-.1175	-.0294
0.8	-1.03	0.2980	0.0432	-.0475	-.0447	-.1117	-.1135	-.0355
1.2	-.938	0.1834	0.0860	-.0763	-.0373	-.1599	-.1146	-.0504
1.6	-.894	0.0688	0.1470	-.1146	-.0333	-.2080	-.1157	-.0636

Table 5. Aerodynamic Coefficients for the MBB A-3 Airfoil

at  $M=0.7$  and  $\alpha=1.2^\circ$

$k_c$	$C_{L\delta}$		$C_{L\alpha}$		$C_{L\beta}$		$C_{m\delta}$		$C_{m\alpha}$	
	Real	Imag	Real	Imag	Real	Imag	Real	Imag	Real	Imag
0.1	.218	.786	7.95	-1.77	4.85	-1.38	.012	-.016	-.154	-.178
0.2	.442	1.31	6.83	-1.53	4.05	-1.50	.038	-.033	-.150	-.327
0.3	.579	1.73	6.17	-1.06	3.56	-1.44	.079	-.054	-.154	-.463
0.4	.626	2.11	5.78	-.535	3.25	-1.33	.145	-.075	-.154	-.605
0.6	.579	2.85	5.35	0.479	2.87	-1.12	.287	-.136	-.150	-.908
0.8	.340	3.62	5.24	1.363	2.66	-.987	.503	-.215	-.150	-1.23
1.2	-.49	5.34	5.39	2.829	2.37	-.827	1.12	-.477	-.210	-1.90
1.6	-1.7	7.35	5.74	3.826	2.05	-.660	1.83	-1.00	-.455	-2.51

$k_c$	$C_{m\beta}$		$C_{n\delta}$		$C_{n\alpha}$		$C_{n\beta}$	
	Real	Imag	Real	Imag	Real	Imag	Real	Imag
0.1	-1.05	-.0514	.00000	-.0044	-.0439	-.0061	-.0828	-.0030
0.2	-1.06	-.0804	.00096	-.0082	-.0399	-.0158	-.0806	-.0080
0.3	-1.08	-.1041	.00337	-.0118	-.0379	-.0258	-.0802	-.0131
0.4	-1.09	-.1267	.00683	-.0153	-.0355	-.0367	-.0800	-.0186
0.6	-1.13	-.1654	.01702	-.0225	-.0299	-.0590	-.0805	-.0293
0.8	-1.17	-.1845	.03175	-.0275	-.0239	-.0814	-.0817	-.0394
1.2	-1.24	-.1257	.07540	-.0457	-.0079	-.1284	-.0848	-.0575
1.6	-1.22	-.1210	.13793	-.0680	0.0073	-.1791	-.0874	-.0729

Table 6. Aerodynamic Coefficients for the MBB A-3 Airfoil  
at  $M=0.74$  and  $\alpha=1.2^\circ$

$k_c$	$C_{L\delta}$		$C_{L\alpha}$		$C_{L\beta}$		$C_{m\delta}$		$C_{m\alpha}$	
	Real	Imag	Real	Imag	Real	Imag	Real	Imag	Real	Imag
0.1	.299	.867	8.90	-2.48	5.25	-1.85	.024	-.004	-.038	-.324
0.2	.603	1.39	7.34	-2.15	4.20	-1.95	.077	-.034	-.098	-.524
0.3	.818	1.80	6.56	-1.60	3.60	-1.85	.121	-.060	-.130	-.707
0.4	.935	2.20	6.18	-1.05	3.22	-1.74	.162	-.129	-.186	-.870
0.6	.945	2.85	5.80	-.109	2.65	-1.54	.291	-.304	-.367	-1.26
0.8	.820	3.46	5.59	0.443	2.22	-1.27	.465	-.463	-.655	1.51
1.2	.186	4.88	5.09	1.787	1.98	-.687	.813	-.768	-.794	1.67
1.6	-.87	6.60	5.10	3.127	1.94	-.470	1.38	-1.16	-.746	-2.09

$k_c$	$C_{m\beta}$		$C_{n\delta}$		$C_{n\alpha}$		$C_{n\beta}$	
	Real	Imag	Real	Imag	Real	Imag	Real	Imag
0.1	-1.13	-.1040	-.0001	-.0038	-.0395	-.0066	-.0824	-.0044
0.2	-1.19	-.1317	.00219	-.0075	-.0371	-.0190	-.0814	-.0103
0.3	-1.24	-.1402	.00555	-.0110	-.0348	-.0310	-.0816	-.0165
0.4	-1.29	-.1324	.01025	-.0148	-.0327	-.0427	-.0825	-.0224
0.6	-1.38	-.0444	.02232	-.0242	-.0287	-.0671	-.0855	-.0330
0.8	-1.33	0.1094	.03931	-.0346	-.0258	-.0933	-.0888	-.0409
1.2	-1.09	0.0468	.08092	-.0576	-.0184	-.1383	-.0900	-.0563
1.6	-1.07	-.0775	.14038	-.0844	-.0035	-.1856	-.0916	-.0733

Table 7. Aerodynamic Coefficients for the MBB A-3 Airfoil  
at  $M=0.765$  and  $\alpha=0.86^\circ$

$k_c$	$C_{L\delta}$		$C_{L\alpha}$		$C_{L\beta}$		$C_{m\delta}$		$C_{m\alpha}$	
	Real	Imag	Real	Imag	Real	Imag	Real	Imag	Real	Imag
0.1	.412	.952	9.72	-3.67	5.60	-2.61	.009	-.043	-.413	-.249
0.2	.782	1.42	7.51	-3.05	3.97	-2.49	.030	-.092	-.411	-.471
0.3	.985	1.78	6.56	-2.48	3.31	-2.31	.070	-.165	-.577	-.546
0.4	1.09	2.08	6.31	-2.13	3.17	-2.26	.099	-.234	-.662	-.641
0.6	1.08	2.65	5.39	-.854	2.42	-1.55	.173	-.348	-.696	-.838
0.8	.856	3.37	5.20	0.022	2.38	-1.29	.308	-.448	-.710	-1.01
1.2	.078	4.78	4.97	1.662	2.13	-.885	.758	-.712	-.658	-1.86
1.6	-.85	6.61	5.20	2.808	2.46	-1.04	1.35	-1.16	-.670	-2.02

$k_c$	$C_{m\delta}$		$C_{n\delta}$		$C_{n\alpha}$		$C_{n\beta}$	
	Real	Imag	Real	Imag	Real	Imag	Real	Imag
0.1	-1.41	-.0011	.00061	-.0020	-.0200	-.0219	-.0739	-.0139
0.2	-1.34	-.0149	.00234	-.0050	-.0105	-.0407	-.0625	-.0301
0.3	-1.41	0.1130	.00807	-.0104	-.0298	-.0424	-.0828	-.0265
0.4	-1.62	0.1910	.01327	-.0154	-.0313	-.0546	-.0882	-.0283
0.6	-1.22	0.1950	.02483	-.0265	-.0314	-.0802	-.0903	-.0360
0.8	-1.15	0.1458	.03950	-.0375	-.0331	-.0991	-.0932	-.0407
1.2	-1.02	0.0460	.08170	-.0567	-.0233	-.1398	-.0947	-.0548
1.6	-1.06	-.0584	.14160	-.0870	-.0069	-.1879	-.0888	-.0693



Table 8. Aerodynamic Coefficients for the MBB A-3 Airfoil  
at  $M=0.78$  and  $\alpha=0.6^\circ$

$k_c$	$C_{L\delta}$		$C_{L\alpha}$		$C_{L\beta}$		$C_{m\delta}$		$C_{m\alpha}$	
	Real	Imag	Real	Imag	Real	Imag	Real	Imag	Real	Imag
0.1	.634	.981	10.2	-5.63	5.76	-3.86	-.07	-.117	-1.22	.4544
0.2	1.01	1.31	7.32	-4.34	3.74	-3.22	-.12	-.163	-.917	.2452
0.3	1.17	1.55	6.06	-3.14	2.87	-2.52	-.13	-.183	-.783	.0354
0.4	1.20	1.80	5.46	-2.21	2.49	-2.01	-.11	-.192	-.707	-.150
0.6	1.06	2.39	4.91	-.773	2.19	-1.34	.009	-.229	-.614	-.498
0.8	.809	3.06	4.73	0.287	2.08	-1.01	.210	-.315	-.584	-.832
1.2	.219	4.62	4.83	1.743	2.00	-.736	.690	-.638	-.643	-1.46
1.6	-.62	6.26	5.02	2.717	1.82	-.574	1.22	-1.15	-.811	-1.97

$k_c$	$C_{m\beta}$		$C_{n\delta}$		$C_{n\alpha}$		$C_{n\beta}$	
	Real	Imag	Real	Imag	Real	Imag	Real	Imag
0.1	-1.85	0.4989	.00491	-.0002	.00378	-.0487	-.0584	-.0342
0.2	-1.57	0.5260	.01081	-.0052	-.0166	-.0595	-.0766	-.0429
0.3	-1.38	0.4967	.01540	-.0120	-.0279	-.0664	-.0886	-.0401
0.4	-1.25	0.4378	.01939	-.0194	-.0337	-.0731	-.0947	-.0385
0.6	-1.09	0.2808	.02898	-.0324	-.0377	-.0869	-.0979	-.0363
0.8	-1.05	0.1559	.04245	-.0437	-.0361	-.1045	-.0978	-.0408
1.2	-1.08	0.0156	.08425	-.0653	-.0232	-.1468	-.0951	-.0568
1.6	-1.08	-.0036	.14710	-.0962	-.0092	-.1964	-.0967	-.0734

## SECTION V

### RESULTS OF FLUTTER ANALYSIS

Unless otherwise specified, the present flutter analysis was based on the following set of common parameters:  $a_h = -0.2$ ;  $x_\alpha = 0.2$ ;  $r_\alpha = 0.5$ ;  $x_\beta = 0.008$ ;  $r_\beta = 0.06$ ;  $\omega_h/\omega_\alpha = 0.3$ ; and  $\mu = 50$ . The Mach numbers considered were 0.7, 0.8, 0.85, and 0.875 for the NACA 64A006 airfoil and 0.7, 0.74, 0.765, and 0.78 for the NBB A-3 airfoil. A flutter analysis of a flat plate with a trailing-edge aileron at  $M = 0.7$  was first performed using the aerodynamic data obtained from the kernel function method and LTRAN2-NLR code. The two sets of curves obtained for  $U^*$  vs.  $\omega_\beta/\omega_\alpha$  by the two methods agreed well with each other (Reference 29).

#### 1. Effect of Frequency Ratios ( $\omega_\beta/\omega_\alpha$ and $\omega_h/\omega_\alpha$ )

The curves for the flutter speed vs.  $\omega_\beta/\omega_\alpha$  ranging from 0 to 2 for three  $\omega_h/\omega_\alpha$  values (0.1, 0.3, and 0.5) and various Mach numbers were obtained for both airfoils and plotted in Reference 29. Only the results for the NACA 64A006 airfoil at  $M = 0.85$  is given here (Figure 4).

The flutter boundaries for the three branches: bending-torsion; bending-aileron; and torsion-aileron can be correlated to those for the corresponding binary cases except in the transition zones. Such correlation was made in the study of subsonic case (Reference 30).

For  $\omega_h/\omega_\alpha = 0.1$  in Figure 4, the flutter speed for the bending-torsion branch increases very slightly with  $\omega_\beta/\omega_\alpha$  and the curve approaches asymptote for  $\omega_\beta/\omega_\alpha \rightarrow \infty$ , which corresponds to the bending-torsion binary flutter value. For  $\omega_h/\omega_\alpha = 0.1$ , the flutter boundaries for the torsion-aileron and bending-aileron branches appear in the regions of  $\omega_\beta/\omega_\alpha < 0.92$  and 0.18, respectively.

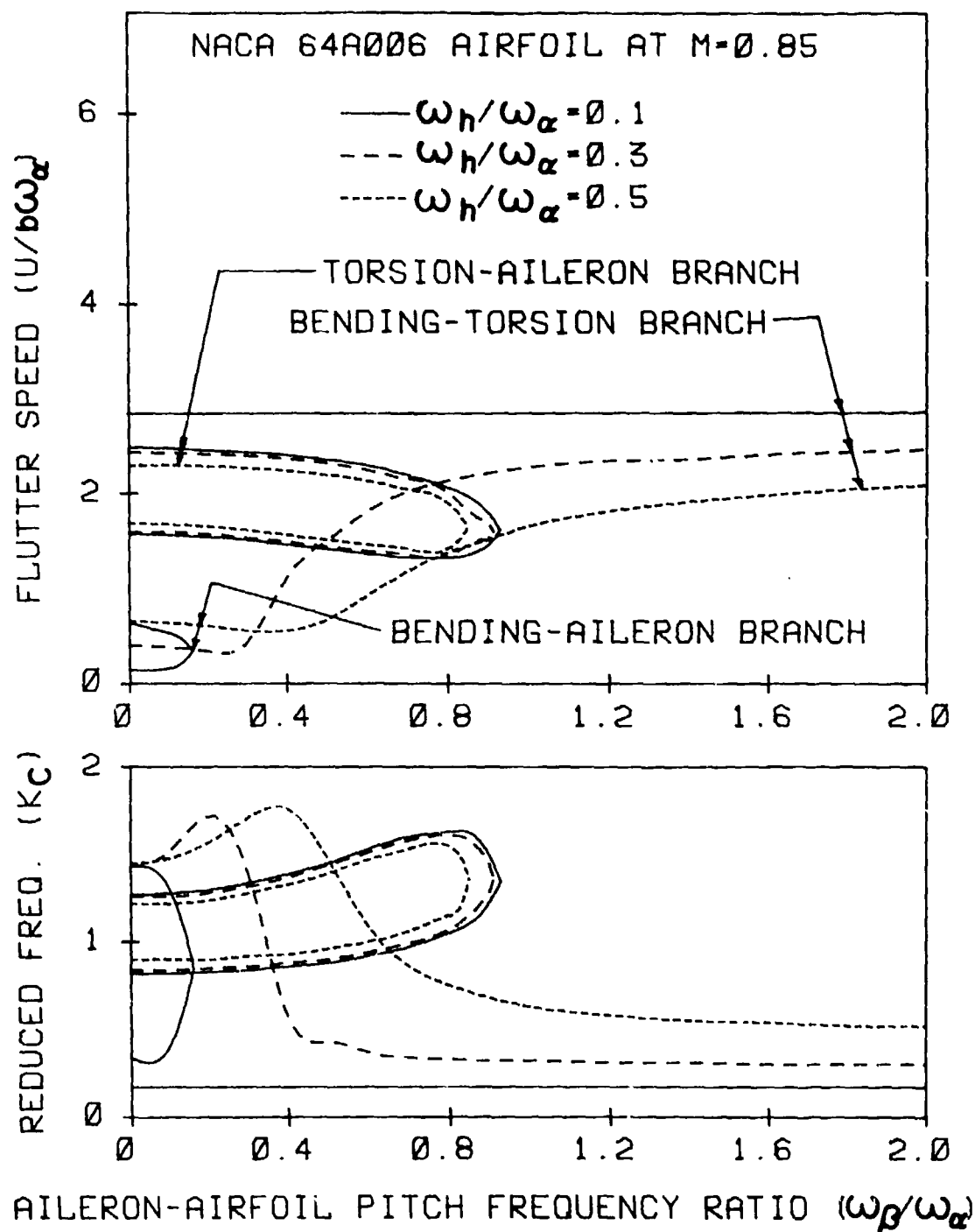


Figure 4 Effect of Aileron-Airfoil Pitch Frequency on Flutter Speed for Three Different Airfoil Plunge-Pitch Frequency Ratios

For  $\omega_h/\omega_\alpha = 0.3$  and  $0.5$ , the flutter boundaries for the torsion-aileron branches are not too much different than those for  $\omega_h/\omega_\alpha = 0.1$ . However, the two boundaries for bending-torsion and bending-aileron branches become continuous curves, each with a transition portion. The resulting curves obtained for all other Mach numbers for both airfoils show the trends similar to those found in Figure 4 of Reference 29.

A common means to eliminate the flutter boundaries for the bending-aileron and the torsion-aileron branches is to use aileron mass balance or high aileron pitch stiffness. For a modern aircraft with power-operated irreversible controls, the value of  $\omega_\beta/\omega_\alpha$  is much higher than, say,  $1.0$  and thus the flutter boundaries for the two aileron associated branches do not exist. In the following analyses,  $\omega_\beta/\omega_\alpha$  values considered were  $0.8$  and  $1.5$ , respectively, such that the flutter boundaries for the bending-aileron branch is totally avoided but the torsion-aileron branch still exists at  $\omega_\beta/\omega_\alpha = 0.8$ .

## 2. Effect of Mass Ratio ( $\mu$ )

The curves for the flutter speed vs. mass ratio  $\mu$  for two  $\omega_\beta/\omega_\alpha$  values,  $0.8$  and  $1.5$ , and various Mach numbers were obtained for both airfoils (Reference 29). Only the results for the MBB A-3 airfoil at the design Mach number  $0.765$  is shown here (Figure 5).

For  $\omega_\beta/\omega_\alpha = 1.5$ , the flutter speed for the bending-torsion branch increases with  $\mu$  in a fashion similar to that for the bending-torsion binary flutter. The flutter boundaries for the two aileron associated branches are absent.

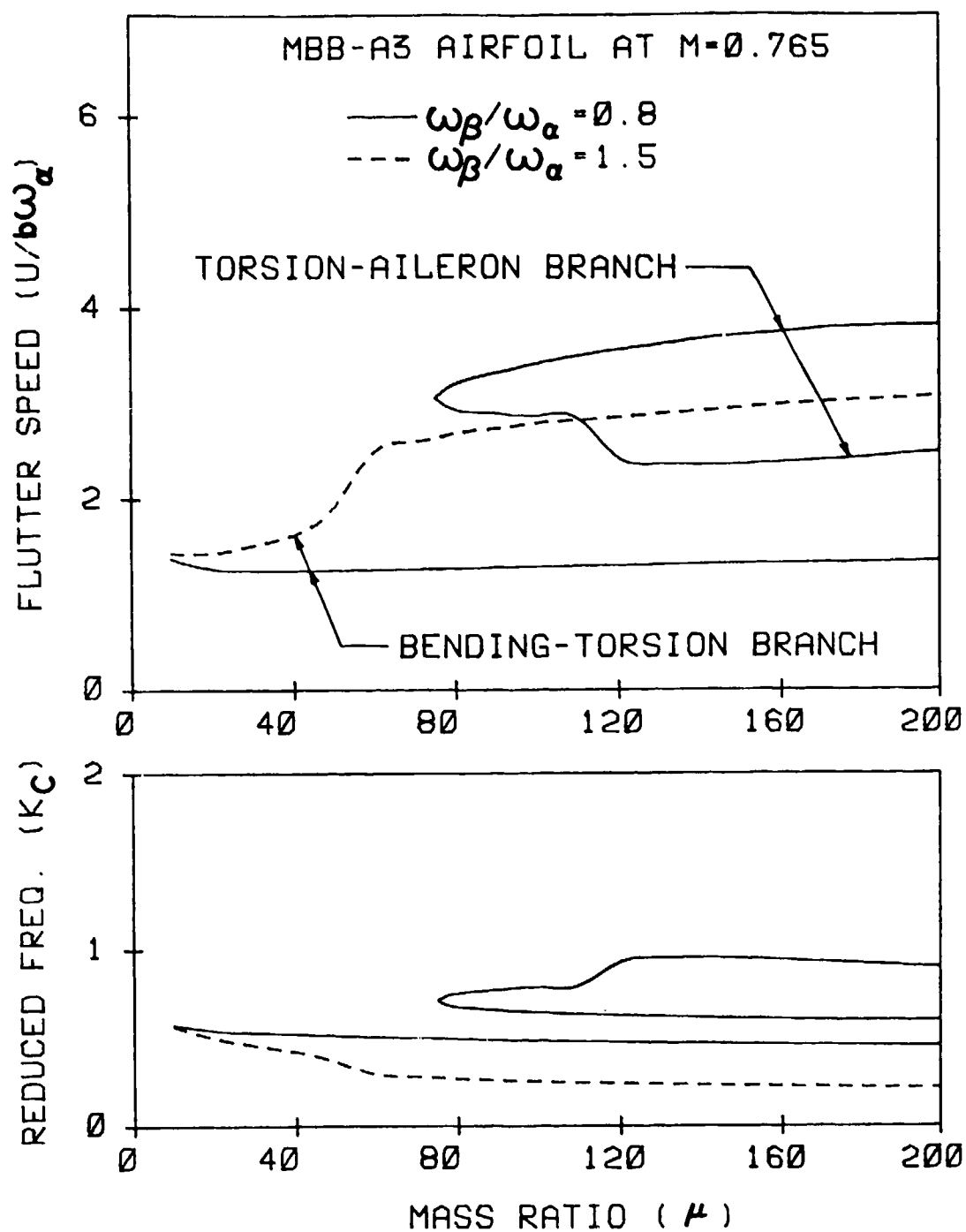


Figure 5 Effect of Mass Ratio on Flutter Speed

For  $\omega_\beta/\omega_\alpha = 0.8$ , the flutter speed for the bending-torsion branch increases with  $\mu$  at a much slower rate than that in the former case, due to the effect of aileron motion. The boundary for the bending-torsion branch is lower than the torsion-aileron branch.

### 3. Effect of the Position of Airfoil Mass Center ( $x_\alpha$ )

The curves for the flutter speed vs.  $x_\alpha$  ranging from -0.2 to 0.4 for two  $\omega_\beta/\omega_\alpha$  values (0.8 and 1.5) were obtained for the MBB A-3 and the NACA 64A006 airfoils at  $M = 0.765$  and 0.85, respectively (Reference 29). Only the results for the MBB A-3 airfoil at the design Mach number 0.765 is shown here (Figure 6).

For  $\omega_\beta/\omega_\alpha = 1.5$ , the flutter speed for the bending-torsion branch increases as the mass center moves forward. The flutter boundary for the torsion-aileron branch only appears when  $x_\alpha < 0$ . The flutter boundary for the bending-aileron branch is absent.

For  $\omega_\beta/\omega_\alpha = 0.8$ , the flutter boundary for the torsion-aileron branch extends to  $x_\alpha = 0.12$ . The boundary for the bending-torsion branch appears at  $x_\alpha > -0.1$ . The last two boundaries become continuous with a transition portion in the neighborhood of  $x_\alpha = 0.1$ .

It is physically clear that when an airfoil oscillates with only a single pitching motion, the forward movement of the mass center stabilizes the airfoil. Such stabilizing effect is also evident in the present flutter speed curves for the bending-torsion branch of a three d.o.f. system.

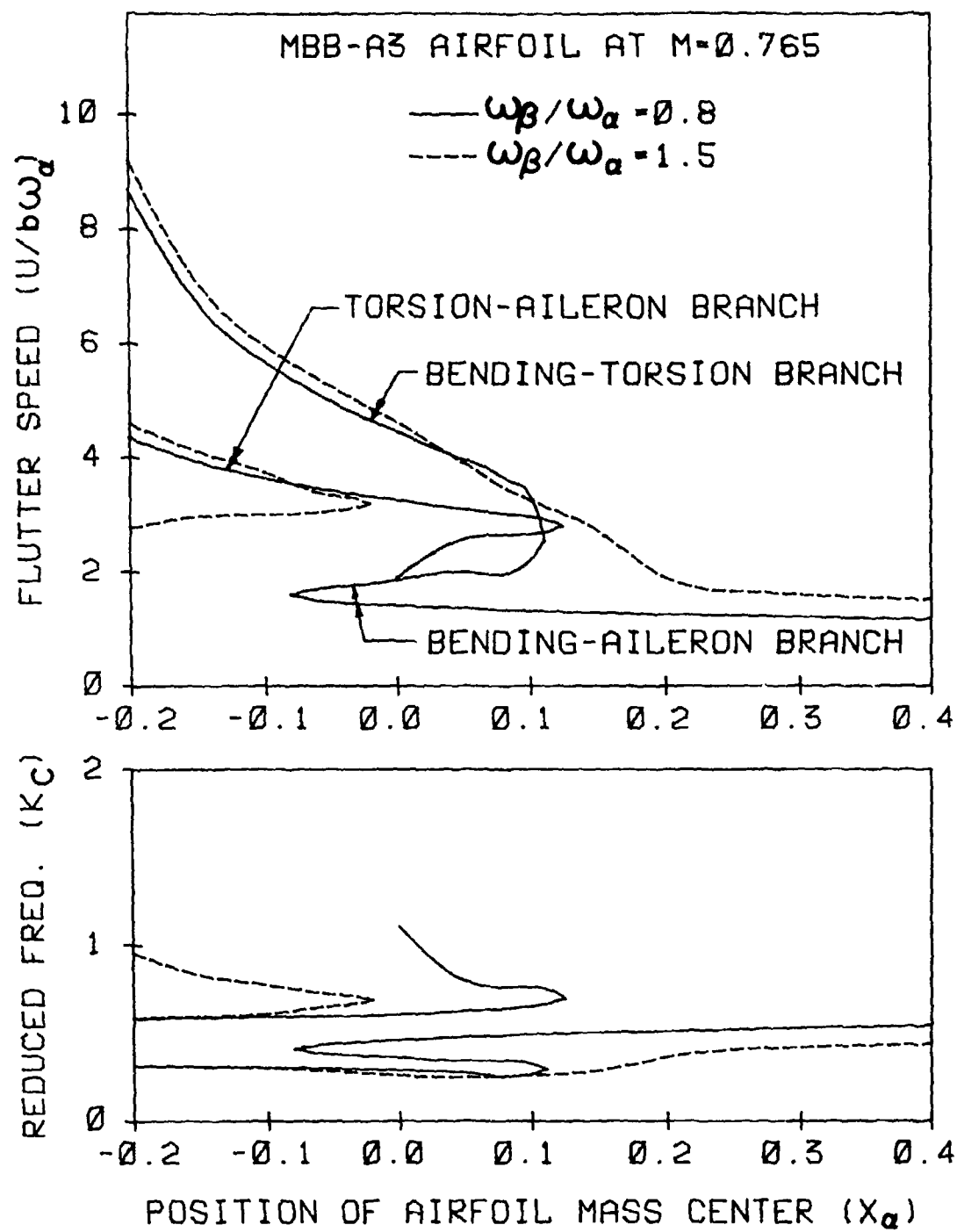


Figure 6 Effect of Position of Airfoil Mass Center on Flutter Speed

#### 4. Effect of the Position of Elastic Axis ( $a_h$ )

The curves for the flutter speed vs.  $a_h$  ranging from -0.5 to 0 for two  $\omega_\beta/\omega_\alpha$  values (0.8 and 1.5) were obtained for the NACA 64A006 and the MBB A-3 airfoils at  $M = 0.85$  and  $0.765$ , respectively (Reference 29). Only the results for the NACA 64A006 airfoil is shown here (Figure 7).

For  $\omega_\beta/\omega_\alpha = 1.5$ , the flutter speed for the bending-torsion branch increases as the elastic axis moves forward. The flutter boundary for the torsion-aileron branch appears in the form of a loop in the region of  $a_h < -0.47$ .

For  $\omega_\beta/\omega_\alpha = 0.8$ , the flutter boundary for the bending-torsion branch assumes a similar trend as that of the former case. The loop-shaped boundary for the torsion-aileron branch extends to  $a_h = -0.14$ . The boundaries for the bending-aileron branch disappear in both cases.

The forward movement of the elastic axis has the same stabilizing effect as that of the mass center. Thus, the trend of the flutter boundaries of the bending-torsion branch observed in Figure 7 is quite similar to that in Figure 6.

#### 5. Effect of the Position of Aileron Mass Center ( $x_\beta$ )

The curves for the flutter speed vs.  $x_\beta$  ranging from 0 to 0.02 for two  $\omega_\beta/\omega_\alpha$  values (0.8 and 1.5) were obtained for the NACA 64A006 and the MBB A-3 airfoils at  $M = 0.85$  and  $0.765$ , respectively (Reference 29). Only the results for the NACA 64A006 airfoil are shown here (Figure 8).

For  $\omega_\beta/\omega_\alpha = 1.5$ , only the flutter boundaries for the bending-torsion branch appear. The flutter speed decreases slightly as  $x_\beta$  increases.



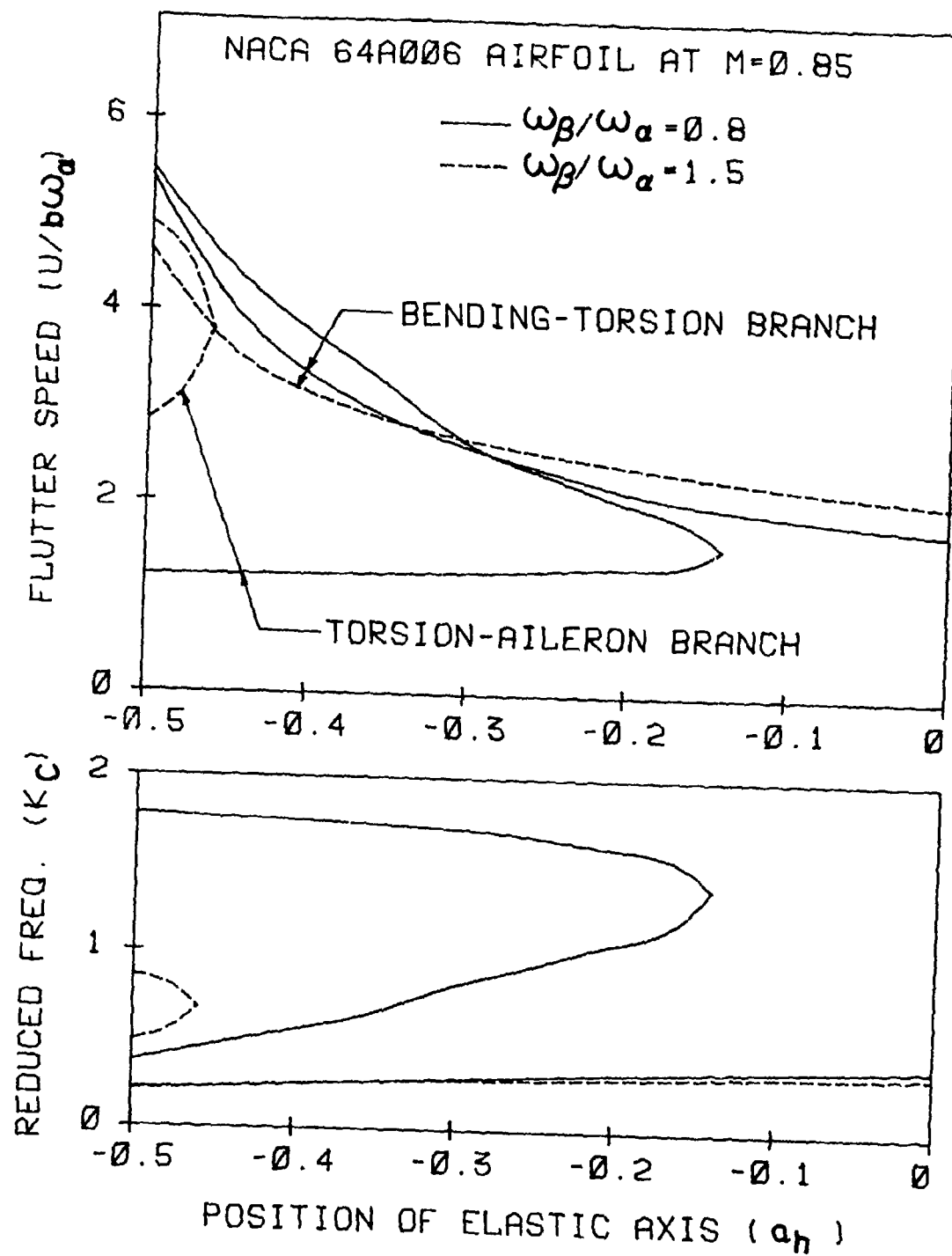


Figure 7 Effect of Position of Elastic Axis on Flutter Speed

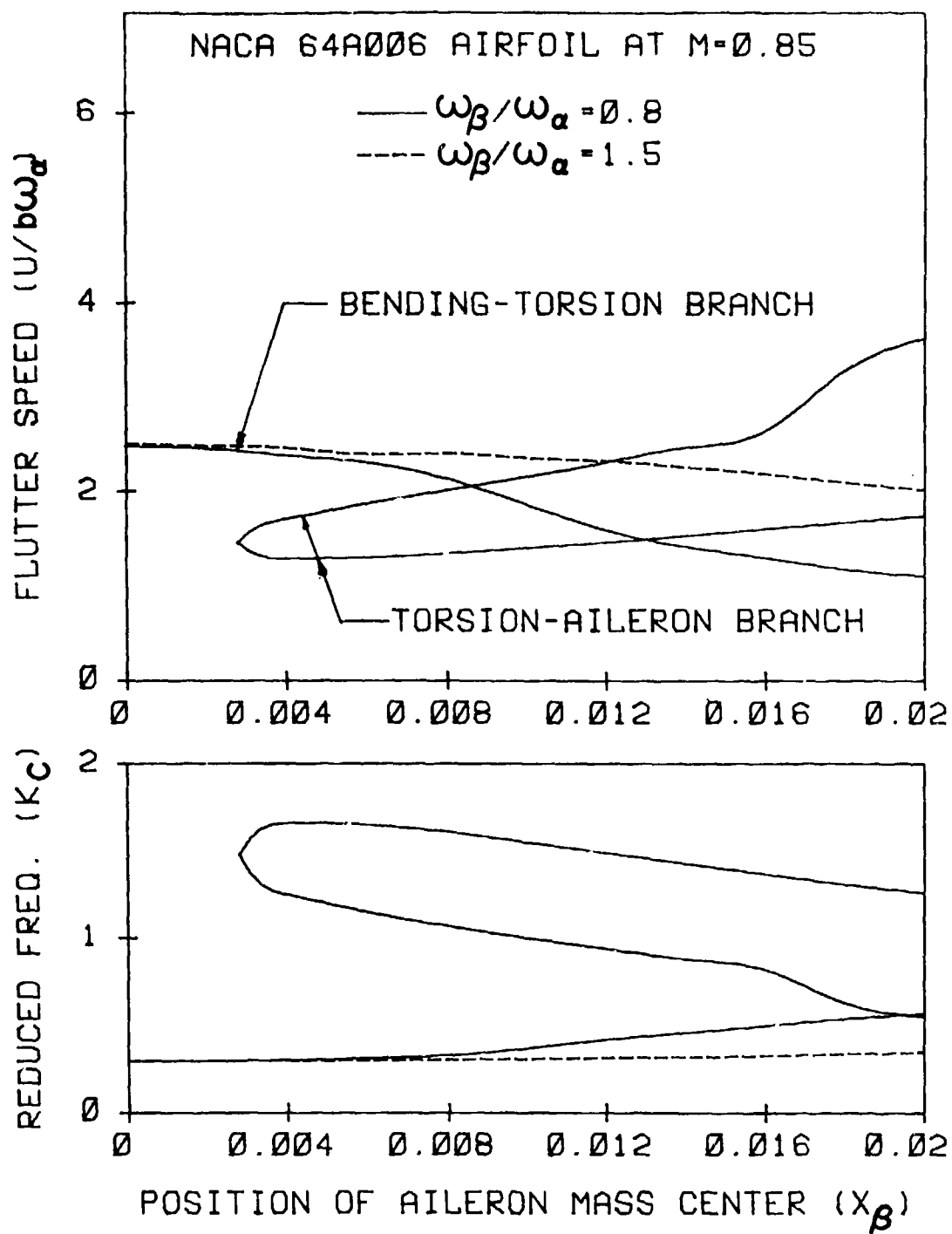


Figure 8 Effect of Position of Aileron Mass Center on Flutter Speed

For  $\omega_\beta/\omega_\alpha = 0.8$ , the decrease in flutter speed for the bending-torsion branch with  $x_\beta$  is more pronounced than that of the former case. The flutter boundary for the torsion-aileron branch appears only at  $x_\beta > 0.004$ . The flutter boundary for the bending-aileron branch is absent.

It may be seen that the forward movement of the aileron mass center can not only eliminate the flutter boundary for the torsion-aileron branch at  $x_\beta < 0.0025$  in this case, but also increase the flutter speed of the bending-torsion branch. The advantage of using aileron mass balance is seen in this case.

#### 6. Effect of Mach Number (M)

Results for the flutter speed vs. Mach number were plotted for both airfoils for  $\mu = 20$  and 50 in Figures 9. The curves were plotted for two values of  $\omega_\beta/\omega_\alpha$ : 0.8 and 1.5. All these curves are for the bending-torsion branch only.

For  $\omega_\beta/\omega_\alpha = 1.5$  and for the present values assumed for the other aeroelastic parameters, only the flutter boundaries for the bending-torsion branch are present. Those for the other two aileron related branches are absent. For  $\omega_\beta/\omega_\alpha = 0.8$ , the flutter boundaries for the bending-aileron branch are absent and those for the torsion-aileron branch are lower than those for the bending-torsion branch. However, the flutter speed curves for the bending-torsion branch at  $\omega_\beta/\omega_\alpha = 0.8$  were still plotted in Figure 9 for the purpose of comparison with those at  $\omega_\beta/\omega_\alpha = 1.5$ . As noted earlier, for a modern aircraft with power-operated irreversible controls the value of  $\omega_\beta/\omega_\alpha$  is much higher than 1.0.

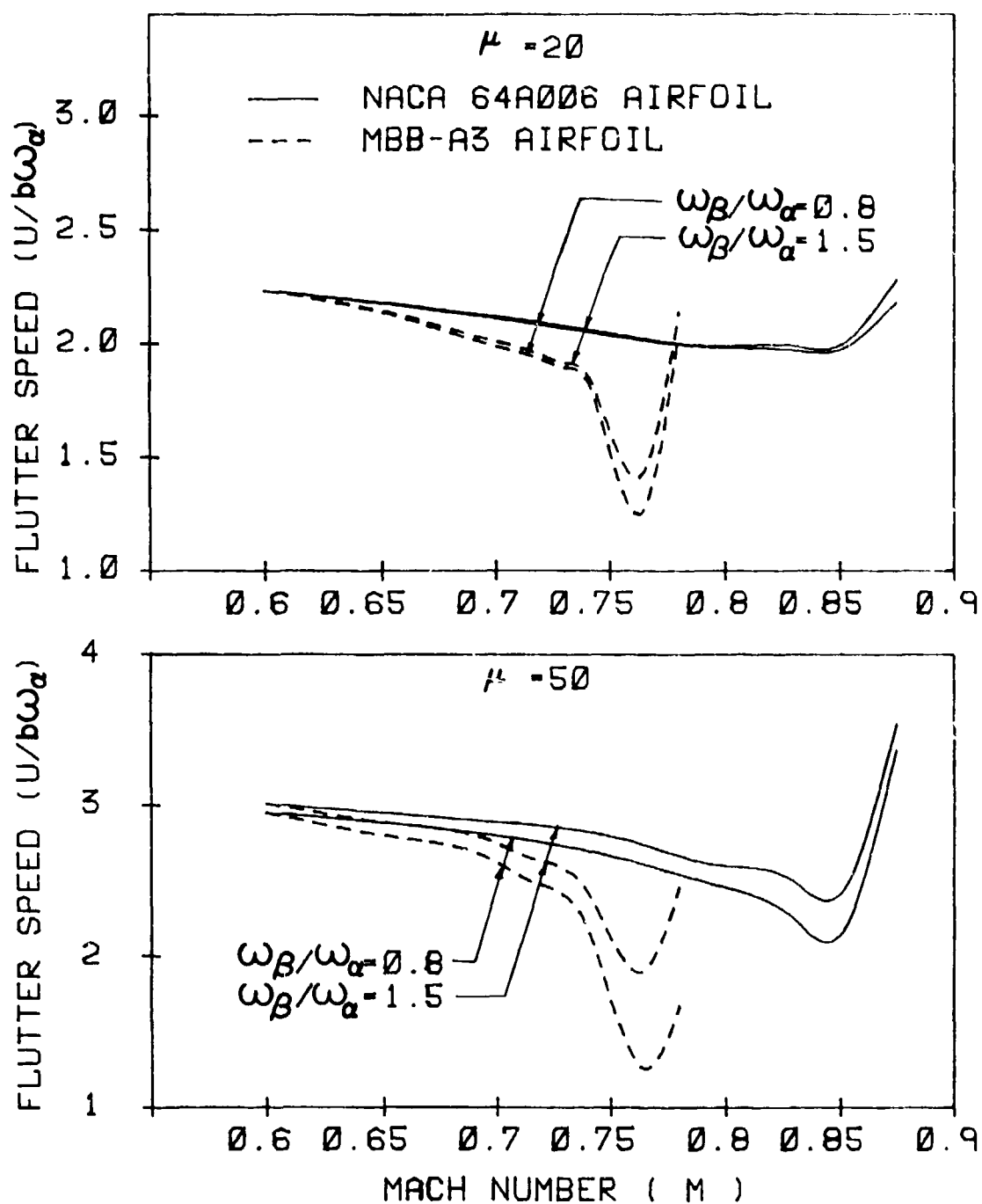


Figure 9 Effect of Mach Number on Flutter Speed for Both Airfoils for Two Mass Ratios:  
 (a)  $\mu=20$  and (b)  $\mu=50$

The figure shows that the bottom of the transonic dip occurs in the neighborhood of the design Mach number of 0.765 for the MBB A-3 airfoil and in the neighborhood of  $M = 0.85$  for the NACA 64A006 airfoil. In a flutter analysis of the NACA 64A006 airfoil with only plunge and pitch d.o.f.'s (Reference 9), the transonic dip for the parameter values considered was also found to be near  $M = 0.85$ .

The figure shows that the mass ratio has a detrimental effect in deepening the transonic dip. This effect was pointed out in Reference 3.

The present examples show that the transonic dips for the MBB A-3 supercritical airfoil are considerably deeper and occur at earlier Mach numbers than those for the NACA 64A006 airfoil. It should, however, be noted that both airfoils are not comparable in configuration.

Results for flutter speed vs. Mach number for other values of the parameters ( $\omega_h/\omega_\alpha$ ,  $x_\alpha$ ,  $a_h$ ) are available in Reference 29.

#### 7. Discussion of the Flutter Modes

To study the flutter mode, the case of two d.o.f.'s (plunge and pitch) was first considered. The flutter speed, plunge-pitch amplitude ratio, and plunge-pitch phase difference were plotted against the mass ratio in Figure 10 for both airfoils and various Mach numbers. The values of the parameters used are the same as those assumed for a NACA 64A010 airfoil in Case A of Reference 12:  $x_\alpha = 1.8$ ;  $r_\alpha = 1.867$ ;  $a_h = -2.0$ ; and  $\omega_h/\omega_\alpha = 1.0$ .

It is seen that, at the bottoms of the transonic dips ( $M = 0.78$  and  $0.875$  for MBB A-3 and NACA 64A006 airfoils, respectively), the amplitude ratios gradually converge to a constant value of 1.868

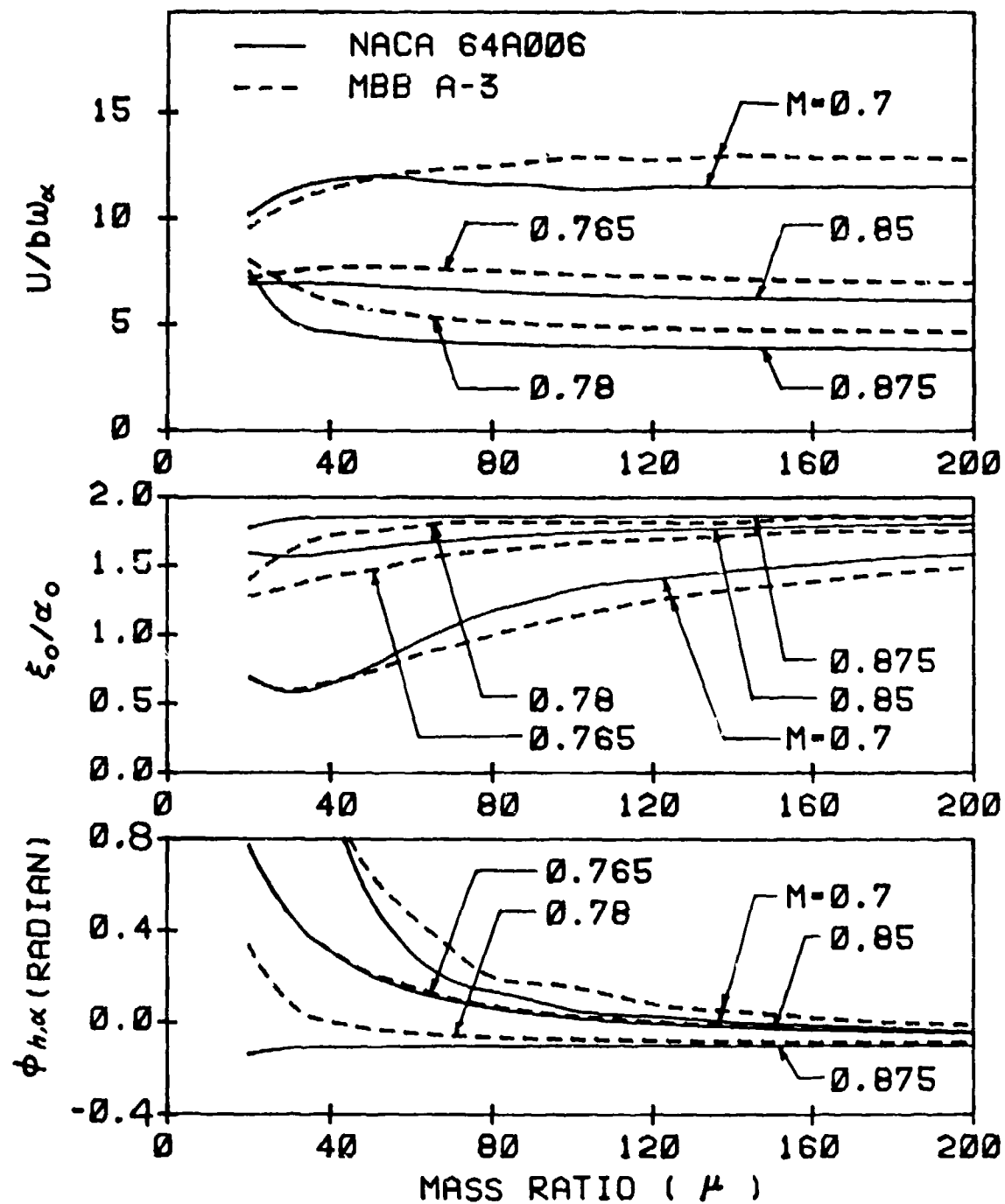


Figure 10 Flutter Speed and Flutter Mode (Amplitude Ratio and Phase Angle) vs. Mass Ratio for Both Airfoils for a Two D.O.F. Case with  $a_h = -2.0$

(first natural mode) and the phase differences gradually approach zero as the mass ratio becomes larger. The phenomenon observed here agrees with that pointed out in Reference 12.

As shown in Figure 11, for the NACA 64A006 airfoil, the two flutter speed curves for  $M = 0.85$  and  $0.875$  cross each other at  $\mu = 185$ . For higher  $\mu$  values, the flutter speed for  $M = 0.875$  becomes increasingly lower than that for  $M = 0.85$  and the bottom of the transonic dip definitely shifts to a Mach number higher than  $0.85$ .

It is seen that for  $M = 0.875$  and  $\mu > 185$ , the amplitude ratio approaches a constant value of  $12.86$  (first natural mode) and the phase difference decreases to zero as  $\mu$  becomes larger.

For the MBB A-3 airfoil, the two flutter curves for  $M = 0.765$  and  $0.78$  cross each other at  $\mu = 195$ . For  $M = 0.78$  and  $\mu > 195$ , the amplitude ratio approaches rather slowly the constant value of  $12.86$  (first natural mode) and the phase difference decreases to zero as  $\mu$  becomes larger.

The MBB A-3 airfoil with three d.o.f.'s is then considered. The parameter values are defined in the first paragraph of this section. It is also defined that  $\omega_\beta/\omega_\alpha = 1.5$ . The results are given in Figure 12.

At  $M = 0.78$ , the plunge-pitch and the plunge-aileron pitch amplitude ratios approach two constant values of  $12.81$  and  $10.1$  respectively (first natural mode) and the two phase differences approach zero as  $\mu$  becomes larger.

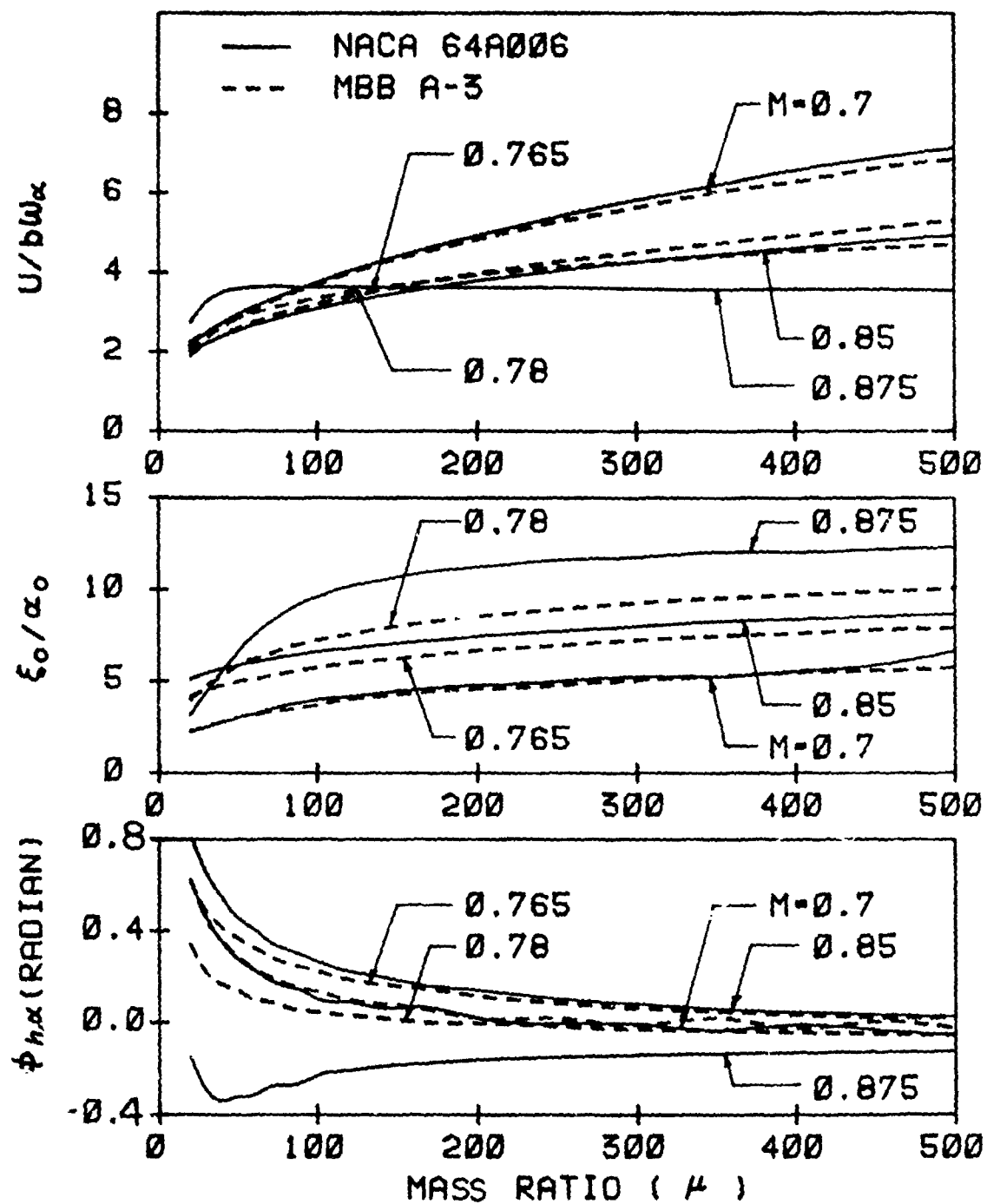


Figure 11 Flutter Speed and Flutter Mode (Amplitude Ratio and Phase Angle) vs. Mass Ratio for Both Airfoils for a Two D.O.F. Case with  $a_h = -0.2$



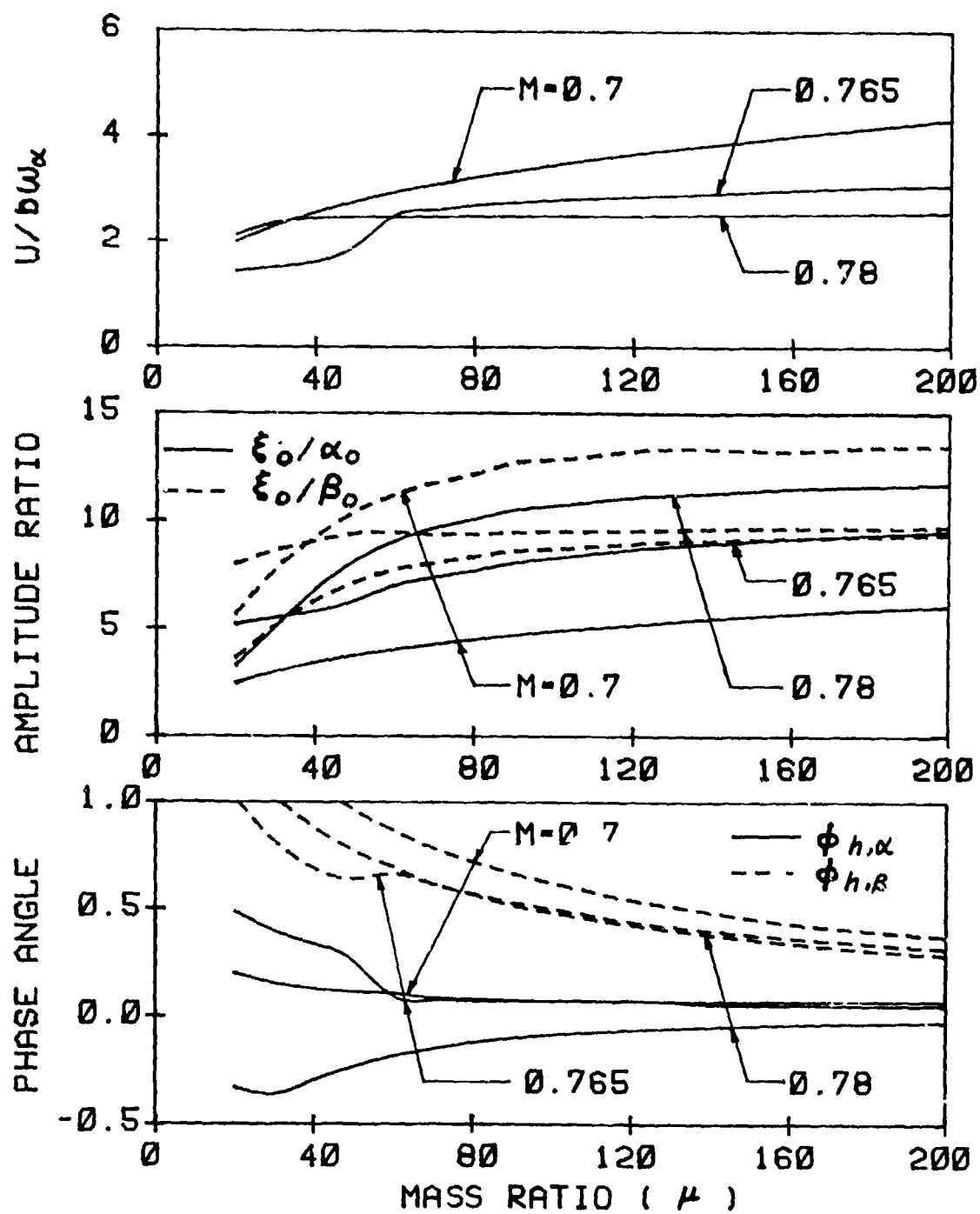


Figure 12 Flutter Speed and Flutter Mode (Amplitude Ratios and Phase Angles) vs. Mass Ratio for the MBB A-3 Airfoil for a Three D.O.F. Case with  $a_h = -0.2$

## SECTION VI

### RESULTS OF TIME RESPONSE ANALYSIS

Time response results were obtained for the NACA 64A006 airfoil at  $M = 0.7$  and  $0.85$  and for the MBB A-3 airfoil at  $M = 0.765$ , respectively. The parameters are defined as:  $a_h = -0.2$ ,  $x_\alpha = 0.2$ ;  $r_\alpha = 0.5$ ;  $x_\beta = 0.008$ ;  $r_\beta = 0.06$ ;  $\omega_h/\omega_\alpha = 0.3$ ;  $\omega_\beta/\omega_\alpha = 1.5$ ; and  $k_c = 0.3$ .

A time-response analysis was first performed for the NACA 64A006 airfoil at  $M = 0.7$ . Based on the flutter speed found in a flutter analysis,  $U^* = 2.816$  at  $\mu = 48$ , the neutrally stable responses were indeed obtained (Reference 29).

A time-response analysis was then performed for the NACA 64A006 airfoil at  $M = 0.85$ . The results for the three displacements and the three aerodynamic forces were plotted in Figures 13 and 14, respectively. In Figure 14,  $c_{\ell_0}$ ,  $c_{m_0}$ , and  $c_{n_0}$  are the amplitudes of  $c_\ell$ ,  $c_m$ , and  $c_n$ , respectively, obtained in the forced harmonic motion.

The airfoil was first forced to oscillate for  $5\frac{1}{2}$  cycles in order for the response of the three aerodynamic coefficients to become periodic. The airfoil was then set free and the aeroelastic time-responses were calculated. Based on a flutter solution,  $U^* = 2.436$  at  $\mu = 52.1$ , the time-responses were found to be slightly diverging (unstable). The flight speed was then reduced by 10% and the time-responses were found to be converging (stable). When the flight speed was reduced by only 4%, the neutrally stable responses were eventually obtained. In the neutrally stable free motion, the frequency was found to be 1% higher than that of the original forcing function.

For the MBB A-3 airfoil at  $M = 0.765$ , the response results for the three displacements and the three aerodynamic forces were plotted in Figures 15 and 16, respectively. In Figure 16,  $dc_\ell$  is the differential

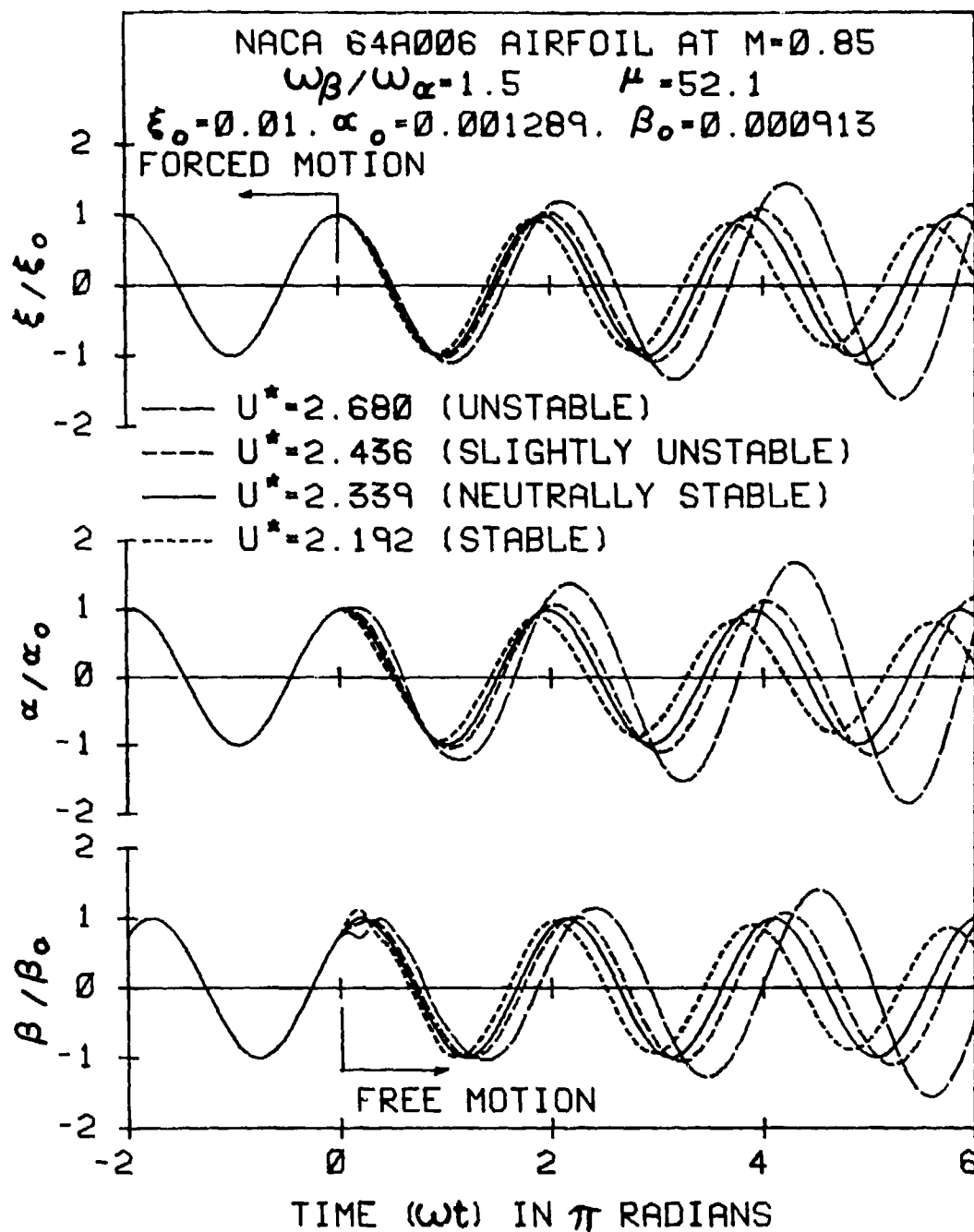


Figure 13 Effect of Flutter Speed on Displacement Responses for the NACA 64A006 Airfoil at  $M = 0.85$

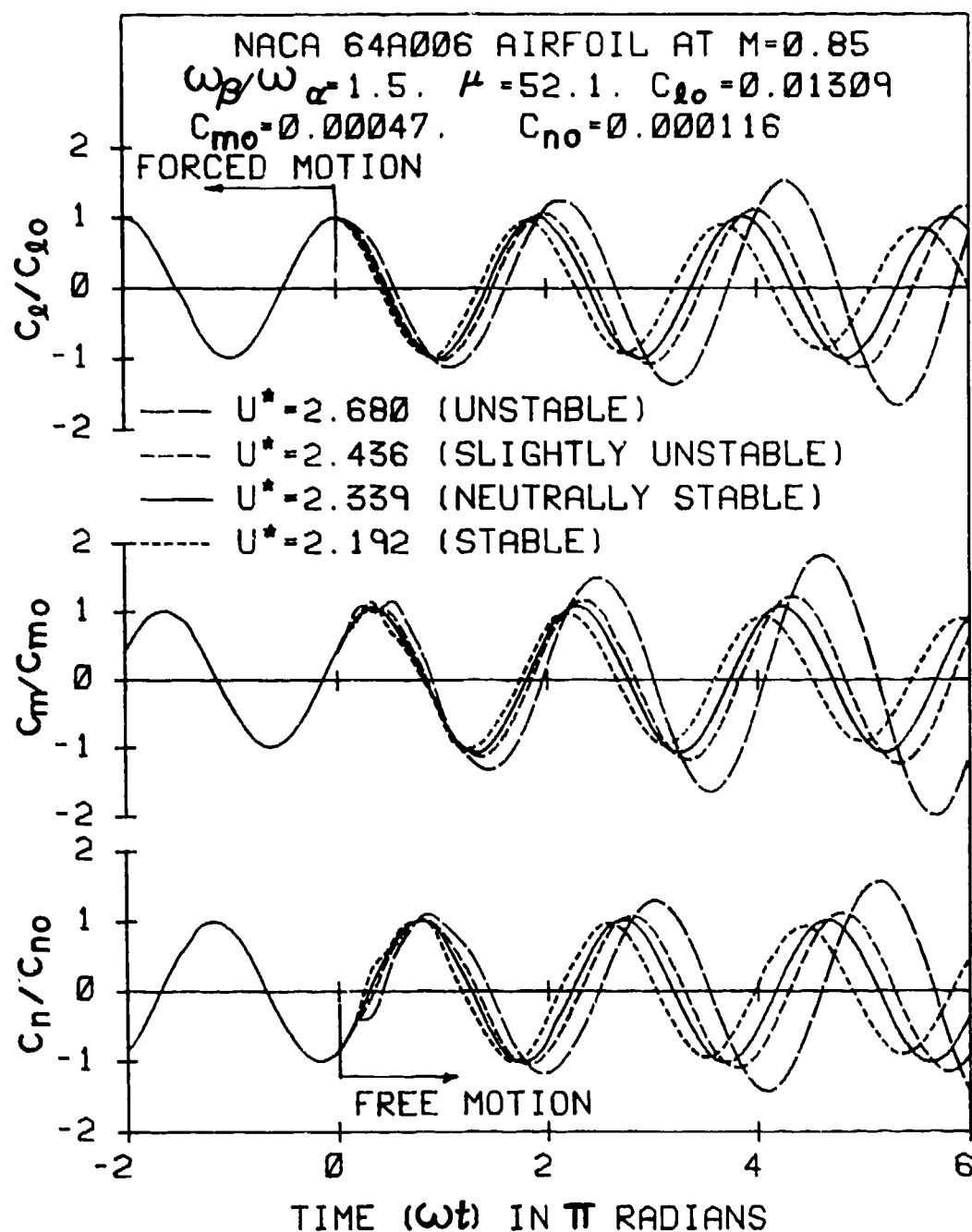


Figure 14 Effect of Flutter Speed on Aerodynamic Responses for the NACA 64A006 Airfoil at  $M = 0.85$

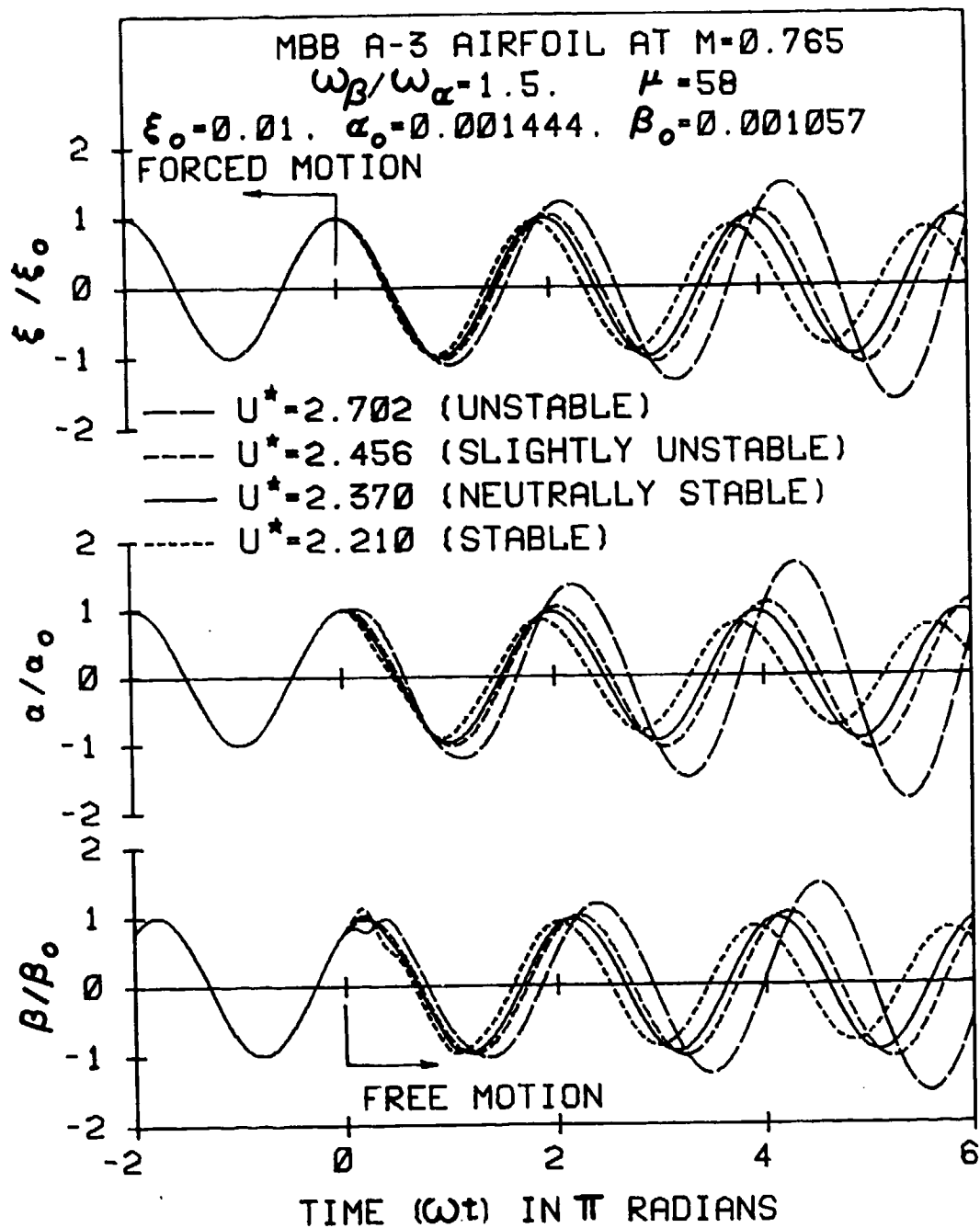


Figure 15 Effect of Flutter Speed on Displacement Responses for the MBB A-3 Airfoil at  $M=0.765$

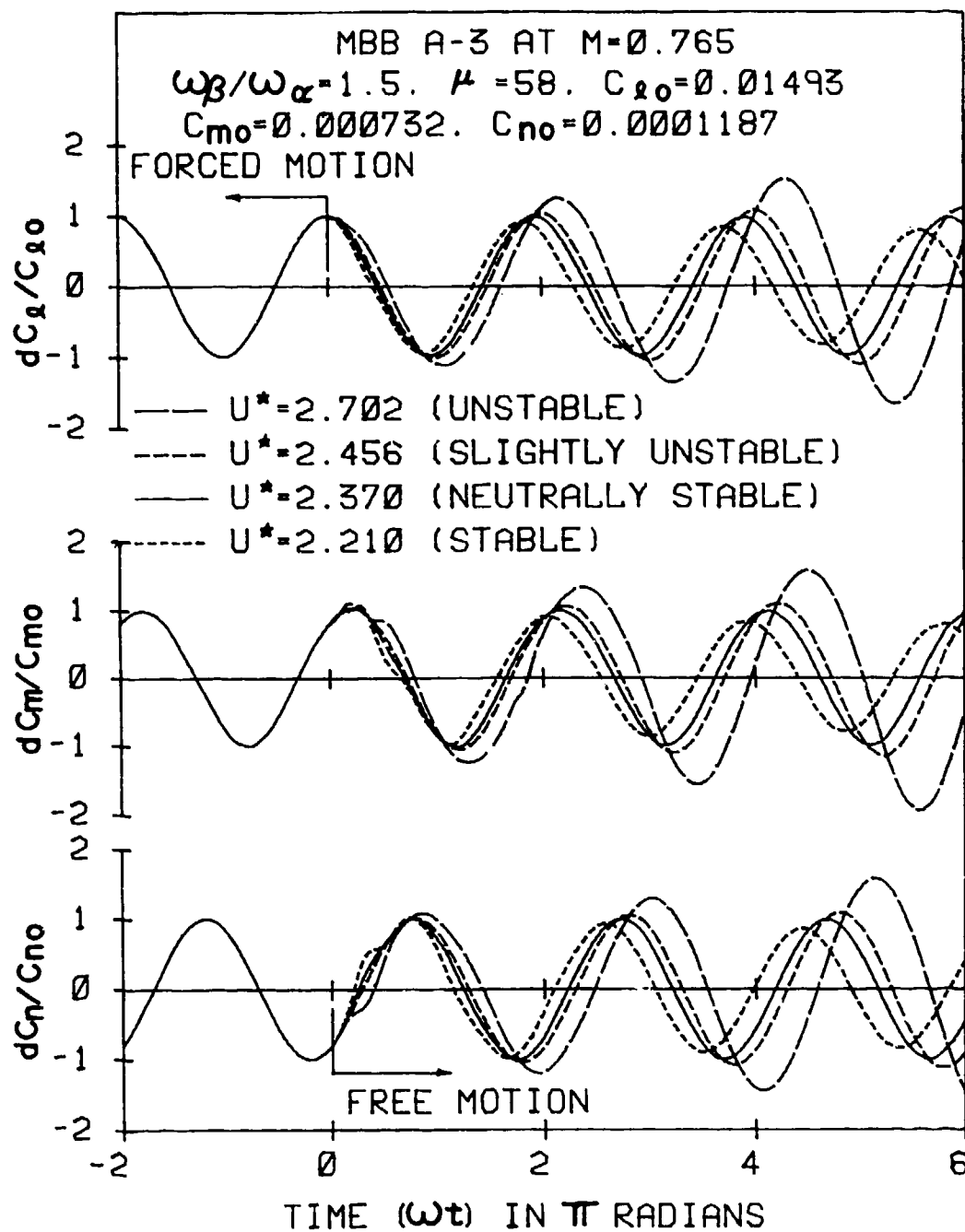


Figure 16 Effect of Flutter Speed on Aerodynamic Responses for the MBB A-3 Airfoil at  $M=0.765$

$c_{\ell}$  relative to the mean value of  $c_{\ell}$  in forced motion;  $dc_m$  and  $dc_n$  are defined in a similar way.

Again, the airfoil was first forced to oscillate for 5 and 1/2 cycles to obtain the periodic aerodynamic responses. Based on a flutter solution,  $U^* = 2.456$  at  $\mu = 58$ , the time-responses were found to be slightly diverging. The neutrally stable responses were obtained when the flight speed was reduced by 3.5%.

## SECTION VII

### CONCLUDING REMARKS

Based on the present flutter and time-response analyses, the following concluding remarks can be made.

(1) As can be seen in Figures 2 and 3, strong shocks are present at  $M = 0.875$  and  $0.78$  for the NACA 64A006 and MBB A-3 airfoils, respectively. Both the steady and unsteady aerodynamic results were obtained by using the LTRAN2-NLR code. Difficulty was, however, encountered when attempting to obtain unsteady results for the NACA 64A006 airfoil at  $M = 0.9$ .

(2) In computing the aerodynamic coefficients for all cases,  $k_c$  values of up to 1.6 were considered. For a flat plate at  $M = 0.7$ , all the nine unsteady aerodynamic coefficients were obtained which agreed reasonably well with the kernel function results (Reference 29).

(3) For the parameter values considered, the results show that the flutter boundaries for the bending-aileron and the torsion-aileron branches generally disappear when  $\omega_\beta/\omega_\alpha$  is greater than one. The aileron effect on flutter speed of the bending-torsion branch diminishes gradually as  $\omega_\beta/\omega_\alpha$  increases.

(4) As seen in Figures 5, 6, and 7, the flutter speed for  $\omega_\beta/\omega_\alpha = 1.5$  increases as the mass ratio becomes larger, as the mass center moves forward, and as the elastic axis moves forward, respectively. It also increases as the radius of gyration of the airfoil becomes larger (Reference 29).



(5) As seen in Figure 8, forward movement of the aileron mass center can not only eliminate the flutter boundaries of aileron associated branches but also increase the flutter speed of the bending-torsion branch.

(6) For the sets of parameter values considered and for the NACA 64A006 and MBB A-3 airfoils at  $M = 0.875$  and  $0.78$ , respectively, each flutter mode converges to its corresponding first natural mode as the mass ratio becomes larger.

(7) For the NACA 64A006 airfoil at  $M = 0.7$ , neutrally stable responses were obtained based on a set of parameter values corresponding to a flutter condition in a separate flutter analysis (Reference 29). For the NACA 64A006 airfoil at  $M = 0.85$  and the MBB A-3 airfoil at  $M = 0.765$ , neutrally stable responses were obtained based on the flight speed 4% and 3.5% lower than the respective flutter speeds found in the separate flutter analyses. Such small differences may mainly be attributed to the use of the principle of linear superposition of airloads in the flutter analyses.

(8) Recently, two-dimensional codes were developed without the restrictions of low-frequency (Reference 12, 19, and 20) and small-disturbance (Reference 21). The viscous effect was accounted for by using a viscous ramp method (Reference 20). Three-dimensional unsteady transonic code has also been developed (Reference 22). These new developments will be very valuable tools for exploring the field of transonic aeroelasticity.

(9) A logical extension of the present development is to include a damping matrix term in the response equations of motion to simulate the active control forces for the application of flutter suppression.

## REFERENCES

1. Ballhaus, W.F. and Bridgeman, J.O., "Numerical Solution Techniques for Unsteady Transonic Problems", AGARD Report No. 679, June 1980, pp. 16-1-16-24.
2. Ashley, H., "Role of Shocks in the 'Sub-Transonic' Flutter Phenomenon", Journal of Aircraft, Vol. 17, March 1980, pp. 187-197.
3. Mykytow, W.J., "A Brief Overview of Transonic Flutter Problems", Unsteady Airloads in Separated and Transonic Flow, AGARD-CP-226, April 1977, pp. 11-1-11-11.
4. Yang, T.Y., Guruswamy, P., and Striz, A.G., "Application of Transonic Codes to Flutter Analysis of Conventional and Supercritical Airfoils", AIAA Paper No. 81-0603, Proceeding of AIAA Dynamics Specialists Conference, Atlanta, GA., April 9-10, 1981, pp. 332-342.
5. Farmer, M.G. and Hanson, P.W., "Comparison of Supercritical and Conventional Wing Flutter Characteristics", Proceedings of AIAA/ASME/ASE 17th Structures, Structural Dynamics, and Materials Conference, King of Prussia, PA., April 1976, pp. 608-614 (also NASA TM X-72837, May 1976).
6. Rizzetta, D.P., "Transonic Flutter Analysis of a Two Dimensional Airfoil", AFFDL-TM-77-64-FBR, July, 1977.
7. Traci, R.M., Albano, E.D., and Farr, J.L., "Small Disturbance Transonic Flows about Oscillating Airfoils and Planar Wings", AFFDL-TR-75-100, June 1975.
8. Ballhaus, W.F. and Goorjian, P.M., "Implicit Finite-Difference Computations of Unsteady Transonic Flows About Airfoils", AIAA Journal, Vol. 15, Dec. 1977, pp. 1728-1735.
9. Yang, T.Y., Guruswamy, P., Striz, A.G., and Olsen, J.J., "Flutter Analysis of a NACA 64A006 Airfoil in Small-Disturbance Transonic Flow", Journal of Aircraft, Vol. 17, April 1980, pp. 225-232.
10. Yang, T.Y., Striz, A.G., and Guruswamy, P., "Flutter Analysis of a Two-Degree-of-Freedom MBB A-3 Supercritical Airfoil in Two-Dimensional Transonic Flow", AIAA Paper No. 80-0736, Proceedings of AIAA/ASME/ASCE/AHS 21st Structures, Structural Dynamics, and Materials Conference, Seattle, WA., May 12-14, 1980, pp. 434-443.
11. Isogai, K., "On the Transonic-Dip Mechanism of Flutter of a Sweptback Wing", AIAA Journal, Vol. 17, July 1979, pp. 793-795.

12. Isogai, K., "Numerical Study of Transonic Flutter of a Two-Dimensional Airfoil", NAL TR-617T, National Aerospace Lab., Tokyo, Japan, July 1980.
13. McGrew, J.A., Giesing, J.P., Pearson, R.M., Zuruddin, K., Schmidt, M.E., and Kalman, T.P., "Supercritical Wing Flutter", AFFDL-TR-78-37, March 1978.
14. Eastep, F.E. and Olsen, J.J., "Transonic Flutter Analysis of a Rectangular Wing with Conventional Airfoil Section", AIAA Journal, Vol. 18, Oct. 1980, pp. 1159-1164.
15. Ballhaus, W.F. and Goorjian, P.M., "Computation of Unsteady Transonic Flows by the Indicial Method", AIAA Journal, Vol. 16, Feb. 1978, pp. 117-124.
16. Rizzetta, D.P., "Time-Dependent Responses of a Two-Dimensional Airfoil in Transonic Flow", AIAA Journal, Vol. 17, Jan. 1979, pp. 26-32.
17. Guruswamy, P. and Yang, T.Y., "Aeroelastic Time Response Analysis of Thin Airfoils by Transonic Code LTRAN2", To appear in Journal of Computers and Fluids.
18. Houwink, R. and van der Vooren, J., "Results of an Improved Version of LTRAN2 for Computing Unsteady Airloads on Airfoils Oscillating in Transonic Flow", AIAA Paper 79-1553, AIAA 12th Fluid and Plasma Dynamics Conference, Williamsburg, VA. July 23-25, 1979.
19. Rizzetta, D.P. and Chin, W.C., "Effect of Frequency in Unsteady Transonic Flow", AIAA Journal, Vol. 17, July 1979, pp. 779-781.
20. Rizzetta, D.P. and Yoshihara, H., "Computations of the Pitching Oscillation of a NACA 64A010 Airfoil in the Small Disturbance Limit", AIAA Paper 80-0128, AIAA 18th Aerospace Science Meeting, Pasadena, CA., Jan. 14-16, 1980.
21. Goorjian, P.M., "Implicit Computations of Unsteady Transonic Flow Governed by the Full Potential Equation in Conservation Form", AIAA Paper 80-0150, AIAA 18th Aerospace Science Meeting, Pasadena, CA., Jan. 14-16, 1980.
22. Borland, C., Rizzetta, D., and Yoshihara, H., "Numerical Solution of Three-Dimensional Unsteady Transonic Flow Over Swept Wings", AIAA Paper 80-1369, AIAA 13th Fluid and Plasma Dynamics Conference, Snowmass, Co., July 14-16, 1980.
23. Fung, Y.C., Theory of Aeroelasticity, Dover Publications, Inc., New York, N.Y., 1969. Sections 6.10 and 6.11.

24. Davis, S.S. and Malcolm, G.N., "Experiments in Unsteady Transonic Flow," AIAA Paper 79-0769, AIAA/ASME/ASCE/AHS 20th Structures, Structural Dynamics and Materials Conference, St. Louis, MO., April 4-6, 1979.
25. Bathe, K.J. and Wilson, E.L., Numerical Methods in Finite Element Analysis, Prentice-Hall, Inc., Englewood Cliffs, N.J., 1976, Chapters 8 and 9.
26. Bland, S.R., "AGARD Two-Dimensional Aeroelastic Configurations," AGARD-AR-156, August 1979.
27. Tijdeman, H., "Investigation of the Transonic Flow Around Oscillating Airfoils," NLR-TR-77090U, National Aerospace Laboratory, The Netherlands, Dec. 1977.
28. Bucciandini, G., Oggiano, M.S., and Onorato, M., "Supercritical Airfoil MBB A-3, Surface Pressure Distributions, Wake and Boundary Condition Measurements," AGARD Advisory Report 138, May 1979, pp. A8-1 to A8-25.
29. Chen, C.H., "Flutter and Time Response Analyses of Three Degree of Freedom Airfoils in Transonic Flow," Ph.D. Thesis, Purdue University, W. Lafayette, IN, July 1981.
30. Theodorsen, T. and Garrick, E.I., "Flutter Calculations in Three Degrees of Freedom," NACA Report 741, 1942.